npj | biofilms and microbiomes

Article

Published in partnership with Nanyang Technological University

https://doi.org/10.1038/s41522-024-00550-4

Hfq-binding small RNA PqsS regulates *Pseudomonas aeruginosa pqs* quorum sensing system and virulence

Tianyuan Jia[1,2,7], Xianbiao Bi[1,2,7], Menglu Li[1,2], Chenhui Zhang[1,2], Anmin Ren[2], Shangru Li[2], Tian Zhou[2], Yingdan Zhang[1,2], Yang Liu[3], Xue Liu[4], Yinyue Deng[5], Bin Liu[6], Guobao Li[1,2] & Liang Yang[1,2]

Pseudomonas aeruginosa is a widespread nosocomial pathogen with a significant to cause both severe planktonic acute and biofilm-related chronic infections. Small RNAs (sRNAs) are noncoding regulatory molecules that are stabilized by the RNA chaperone Hfq to trigger various virulence-related signaling pathways. Here, we identified an Hfq-binding sRNA in *P. aeruginosa* PAO1, PqsS, which promotes bacterial pathogenicity and *pseudomonas quinolone signal* quorum sensing (*pqs* QS) system. Specifically, PqsS enhanced acute bacterial infections by inducing host cell death and promoting rhamnolipid-regulated swarming motility. Meanwhile, PqsS reduced chronic infection traits including biofilm formation and antibiotic resistance. Moreover, PqsS repressed *pqsL* transcript, increasing PQS levels for *pqs* QS. A PQS-rich environment promoted PqsS expression, thus forming a positive feedback loop. Furthermore, we demonstrated that the PqsS interacts and destabilizes the *pqsL* mRNA by recruiting RNase E to drive degradation. These findings provide insights for future research on *P. aeruginosa* pathogenesis and targeted treatment.

Pseudomonas aeruginosa is an opportunistic pathogen that is prevalent in hospital environments[1]. This bacterium is one of the most commonly isolated pathogens and is responsible for high rates of morbidity and mortality in patients worldwide[2]. Indeed, *P. aeruginosa* infections are responsible for a large number of hospital-acquired cases of chronic infections (such as implants, intubation, and cystic fibrosis) and acute infections (such as pneumonia and bacteremia)[3]. *P. aeruginosa* chronic colonization is associated with high-density biofilm formation with matrix-enclosed aggregates that are difficult to eliminate[4]. Under specific environmental conditions, *P. aeruginosa* disperses from the initial infection site to other parts of the body, leading to acute systemic dissemination. A series of virulence factors are released during *P. aeruginosa* infections, such as LasB elastase, and rhamnolipids (RLs)[5]. Among them, RLs are involved in mediating the swarming motility[6]. The expression of these virulence factor is controlled by quorum sensing (QS) systems, two-component systems, and cyclic diguanosine monophosphate (c-di-GMP) signaling[7]. Four interconnected QS systems, *las*, *rhl*, *pqs*, and *iqs*, control collective behaviors in a bacterial population and signal molecules in a density-dependent manner to regulate bacterial pathogenicity during infections[8].

Pseudomonas quinolone signal, 2-heptyl-3-hydroxy-4 (1H)-quinolone (PQS), is the signaling molecule of the *pqs* QS system, specifically secreted by *Pseudomonas* species[9]. The *pqs* QS system is subject to positive autoinduction because the LysR-type transcriptional regulator PqsR (MvfR) binds to the promoter region of *pqsABCDE* (P*pqsA*), triggering transcription once activated by PQS. The precursor 2-aminobenzoylacetate (2-ABA) is first converted into 2-heptyl-4-quinolone (HHQ) and then transformed into PQS. In addition, 2-ABA is also converted into 2-n-heptyl-4-hydroxyquinoline-N-oxide (HQNO) by the mono-oxygenase PqsL[10]. PQS and HQNO are typically produced at similar levels in *P. aeruginosa* PAO1, but deletion of *pqsL*

[1]Shenzhen National Clinical Research Center for Infectious Disease, Shenzhen Third People's Hospital, The Second Affiliated Hospital of Southern University of Science and Technology, Shenzhen, China. [2]Department of Pharmacology, Joint Laboratory of Guangdong-Hong Kong Universities for Vascular Homeostasis and Diseases, School of Medicine, Southern University of Science a-nd Technology, Shenzhen, China. [3]Medical Research Center, Southern University of Science and Technology Hospital, Shenzhen, China. [4]Department of Pharmacology, Guangdong Key Laboratory for Genome Stability and Human Disease Prevention, International Cancer Center, Shenzhen University Health Science Center, Shenzhen, China. [5]School of Pharmaceutical Sciences (Shenzhen), Shenzhen Campus of Sun Yat-sen University, Sun Yat-sen University, Shenzhen, China. [6]National Key Laboratory of Intelligent Tracking and Forecasting for Infectious Diseases, TEDA Institute of Biological Sciences and Biotechnology, Nankai University, Tianjin, China. [7]These authors contributed equally: Tianyuan Jia, Xianbiao Bi.
e-mail: yangl@sustech.edu.cn

can lead to the overproduction of PQS[11]. At high cell densities, large amounts of PQS signaling molecules can be detected in the bacterial culture supernatant[12] and play multiple roles in *P. aeruginosa* virulence and biofilm formation[13]. For example, PQS causes the death of the host *Caenorhabditis elegans* and disrupts the intestine epitheliumin in mice[14]. In addition, the cell division factor, ZapE, regulates biofilm formation by influencing PQS productions[15]. Bacterial membrane vesicles (MVs) are nanoscale vesicle structures that carry various hydrophobic molecules, proteins, and nucleic acids[16], and have been identified as essential components of the extracellular matrix in biofilms[17,18]. PQS also contributes to *P. aeruginosa* MV formation and is frequently detected in MVs[19,20].

Bacterial small RNAs (sRNAs), particularly trans-encoded sRNAs, are non-coding regulatory molecules that are typically 50–500 nucleotides long and participate in various biological processes in bacteria[21]. sRNAs regulate their targets through multiple mechanisms, such as transcriptional or translational termination, in response to various environmental signals, including phosphate and ammonium[22,23]. The major bacterial RNA-binding protein host factor required for bacteriophage Qβ RNA replication (Hfq), a member of the ubiquitous Lsm/Sm protein family, binds to various sRNAs for stabilization and recognition of target mRNAs[24,25]. The roles of various important *P. aeruginosa* sRNAs participating in infection mechanisms, such as QS, type three secretory system (T3SS), and biofilm formation, have been thoroughly investigated[26,27]. For example, the sRNA PhrS activates quinolone synthesis through PqsR and enhances the *pqs* QS system under low-oxygen conditions[28]. Another *P. aeruginosa* sRNA, PrrF, was required for PQS production and bacterial virulence in response to low-iron conditions in a murine model of acute lung infection[29].

In this study, we aimed to investigate the Hfq-binding sRNA, *P. aeruginosa pqs* QS regulating sRNA (PqsS), in *P. aeruginosa* PAO1 pathogenesis and to elucidate the molecular mechanisms underlying its regulatory pathways. We showed that PqsS promoted bacterial acute infections, while repressed biofilm-related chronic infection traits. PqsS repressed PqsL to reduce HQNO production and facilitate PQS production for *pqs* QS system and MVs formation, while PQS-rich environment further promotes PqsS expression, thus forming a positive feedback loop. Specifically, PqsS interacted with and destabilized the *pqsL* mRNA by recruiting RNase E to drive degradation.

Methods

Bacterial growth and cell culture

P. aeruginosa strains, plasmids, and primers used in this study are provided in Supplementary Table 1. Bacteria were cultured in tryptic soytone broth (TSB) (1.7% tryptone, 0.3% soytone, 0.25% glucose, 0.5% NaCl, 0.25% K_2HPO_4), Luria–Bertani (LB) broth (1% tryptone, 0.5% yeast extract, 0.5% NaCl), or ABTGC B-medium (0.1% $MgCl_2$, 0.1% $CaCl_2$, 0.1% $FeCl_3$) supplemented with 10% A10, 0.2% glucose, and 0.2% casamino acids. The media was solidified with 1.5% Bacto Agar (Difco, USA). The overnight-grown subcultures were transferred into 96-well plates, and their growth curves were measured for cell density analysis (OD_{600}) for 24 h using a Tecan Spark plate reader (Tecan Group Ltd., Switzerland). To assess whether different PQS concentrations affected PqsS expression, we generated different PQS concentrations TSB medium (1, 10, and 100 μM, respectively) by supplementing PQS-free TSB with PQS. After overnight culture, PAO1 WT bacteria was collected and washed existing PQS by PBS, then add new medium with different PQS concentrations for to treating 1 h. For cell culture, the murine RAW 264.7 (ATCC®TIB-71™) and human A549 (ATCC®CCL-185) cell lines were grown in DMEM medium supplemented with 10% fetal bovine serum (Gibco, USA), and incubated at 37 °C in a 5% CO_2, humidified incubator.

P. aeruginosa mutant, knockdown (KD), and complement strains construction

P. aeruginosa PAO1 deletion mutant strains were generated by homologous recombination. Briefly, the mutants were constructed by overlapping PCR to contain a gentamicin-resistance cassette. The mutant fragments were inserted into pK18, a suicide vector, to produce gene knockout plasmids. Each knockout plasmid was transformed into *E. coli* strain RK600 and conjugally transferred from RK600 to PAO1. The resultant integrants were selected on agar containing 60 μg/mL gentamicin (Gm60). To resolve merodiploids, the Gm-resistant colonies were streaked to produce single colonies on LB+Gm60 plates containing 10% sucrose. Potential mutants without gentamicin-resistance cassettes were screened by PCR using corresponding flanking primers and were confirmed by Sanger sequencing. *P. aeruginosa* PA14 *pqsS* gene knockdown (KD) strains were generated by Clustered Regularly Interspaced Short Palindromic Repeats. The IPTG-inducible system driving dCas9 in pUC18-mini-Tn7T-Plac-dCas9 was replaced with a tetracycline-inducible system for better performance in *P. aeruginosa*, resulting in plasmid pSZU368. pSZU368 was constructed with an sgRNA targeting *pqsS*. Transformation of pSZU368-sgRNA*pqsS*into*P. aeruginosa* PA14 was achieved by tri-parental mating. Complement strains were constructed as follows: Δ*pqsS* + : Δ*pqsS* mutant expressing *pqsS* from a rescue construct using the pMiniCTX1-*pqsS* plasmid 's own promoter; Δ*pqsS* + pJV300-*pqsS*: a promoter-free pJV300 plasmid using the *pqsS* promoter.

RNA isolation and RNA-seq

Bacterial strains were grown in TSB/ LB until the exponential phase. Then, total RNA was isolated using an EASYspin Plus bacterial microRNA kit (Aidlab, China) and purified using a Ribo-Zero rRNA Removal Kit (Epicentre Biotechnologies, USA). The RNA integrity was determined by TapeStation RNA ScreenTape with RNA size distributions. For Nanopore RNA-seq, total RNA was tailed with poly(A) using E. coli Poly(A) Polymerase (NEB, UK). Then, nanopore RNA-seq was performed using a Ligation Sequencing Kit (SQK-LSK109) with an ONT Barcoding Expansion Kit (EXP-NBD114). Artemis was used to show the mapping profiles of our RNA-seq results[30]. For Illumina RNA-seq, The libraries of RNA samples were generated using NEBNext R Ultra™ Directional RNA Library Prep Kit for Illumina R (NEB, USA). The libraries were sequenced using an Illumina Hiseq platform to generate paired-end reads. P. aeruginosa RNA-seq data analysis was performed as previously reported[31].

Northern blotting

Northern blotting was performed using the NorthernMax Kit (Invitrogen, USA). After RNA extraction, 5 μg of total RNA was separated on a 1.2% agarose gel containing formaldehyde. The gels were then electro-blotted onto Brightstar Plus nylon membranes (Applied Biosystems, USA) and immobilized at 85 °C for 30 min. The specific biotin-labeled single-stranded DNA probes (Supplementary Table 1) with optimized concentrations were added to fresh hybridization buffer, and the blots were incubated with a hybridization buffer overnight. 5S rRNA was used as an internal control. After washing, the blots were further washed with Wash and Block Buffer, and then the signal was detected using the biotin chemiluminescence detection kit (Beyotime, China). Hybridization signals were visualized on an Amersham Imager 680. FIJI/ImageJ software was used to measure band intensities.

Fluorescent primer extension

A 6-carboxyfluorescein (FAM)-labeled oligonucleotide complementary to the sequence 99 to 135 bp downstream *pqsS* transcription start site (TSS) was used for primer extension reactions. Total RNA (2 μg) and 1 μM FAM-labeled primer were incubated at 70 °C for 5 min, before reverse transcription at 42 °C for 60 min. The samples were then incubated with 20 μg RNase A at 37 °C for 30 min, after which cDNA was ethanol precipitated and dissolved in 15 μL nuclease-free water. Finally, the products were analyzed on an ABI 3730 genetic analyzer.

RNA In vitro transcription (IVT), protein purification and protein-RNA EMSA

DNA templates were transcribed into PqsS RNA using a T7 High-Efficiency Transcription Kit (TransGen, China). The purified RNA was checked on an 8% Tris-Acr-Urea gel. *P. aeruginosa* Hfq protein was purified as described previously[24]. The PqsS sRNA was in vitro transcribed. For electrophoretic mobility shift assay (EMSAs), a 4 μM stock of Hfq was prepared in binding buffer (20 mM Tris-HCl pH 8.0, 40 mM NaCl, 10 mM KCl, 1 mM $MgCl_2$), and 20 μM stocks of the RNAs were prepared in DEPC water (RNase free). The RNAs were incubated at 50 °C for 3 min before the proteins were added. Native PAGE (8%) was used to study complex formation. Hfq was titrated into PqsS RNAs at different ratios. The RNA concentration was kept constant at 2 μM. After 15 min of incubation at 37 °C, the samples were mixed with 5×EMSA loading buffer (50% v/v glycerol, 50% v/v binding buffer, 5 mM DTT), before loading onto the gel. The gels were run at 4 °C in 1×TBE running buffer and stained with SYBR gold.

Molecular docking

The Hfq PDB structure file was extracted from 7OGM (RCSB PDB ID) by ChimeraX (UCSF)[32]. PqsS sRNA was modified and docked with Hfq by Hdock server[33]. Pymol 1.4 (Schrodinger, LLC) was used to map the interactions between protein and potential ligand[34]. The distance of hydrogen bonds between molecules less than 4.0 Å was recognized as interactive molecules.

Cell death and adhesion assay

Mid-log phase bacteria (OD600 = 0.6) grown in LB broth were centrifuged and resuspended in PBS to infect RAW264.7 murine macrophages or A549 human lung epithelial cells grown in DMEM medium supplemented with 10% FBS at an MOI of 100. After centrifugation of 24-well culture plates, bacterial phagocytosis by macrophage was allowed to proceed for 30 min before washing three times with sterile PBS and adding fresh DMEM media supplemented with 400 μg/mL gentamicin. For cell death assay, after 2 h infection, the culture supernatants were collected for detection of LDH activities. The LDH activities were detected by using a commercial LDH cytotoxicity kit (Yeasen Bio, China) according to standard procedures. For cell adhesion assay of bacteria on A549 human lung epithelial cells, after 2 h infection, unadhered bacteria were washed by PBS and cells were lysis with 1% Triton. Adhered bacteria were plated on LB agar plates. The percent adherence of PAO1 WT, Δ*pqsS*, and Δ*pqsS*+ strains was compared to inocula by plate counts. All the assays were performed in triplicate. Mid-log phase bacteria (OD600 = 0.6) grown in the LB broth were centrifuged and resuspended in phosphate-buffered saline (PBS) to infect RAW264.7 murine macrophages or A549 human lung epithelial cells grown in Dulbecco's Modified Eagle Medium (DMEM) supplemented with 10% FBS at an multiplicity of infection of 100. After centrifugation of 24-well culture plates, bacterial phagocytosis by macrophage was allowed to proceed for 30 min before washing thrice with sterile PBS and adding fresh DMEM media supplemented with 400 μg/mL gentamicin. For the cell death assay, culture supernatants were collected 2 h after infection of LDH activity. LDH activity was detected using a commercial LDH cytotoxicity kit (Yeasen Bio, China), according to standard procedures. For the cell adhesion assay of bacteria on A549 human lung epithelial cells, after 2 h of infection, unadhered bacteria were washed with PBS, and cells were lysed with 1% Triton. Adherent bacteria were plated onto Luria Broth (LB) agar plates. The percent adherence of PAO1 WT, Δ*pqsS*, and Δ*pqsS*+ strains was compared to inocula by plate counts. All assays were performed in triplicate.

Galleria mellonella larva infection model

Fifth-stage *G. mellonella* (wax moth) larvae (Huiyude Bio, China) that were bright and white without gray-black spots with a limited mass ranging from 250 to 350 mg were randomly placed in groups of 20 and starved for 12 h before injection. *P. aeruginosa* PAO1 WT, Δ*pqsS*, and Δ*pqsS*+ strains were grown overnight in the LB liquid media at 37 °C and 220 rpm. Overnight cultures were diluted 1:100 in fresh LB broth and grown to an OD_{600} of 0.8. Cultures were centrifuged, washed in sterile PBS, and resuspended at an OD_{600} of 0.1. Serial dilutions were prepared in PBS to a final concentration of 5000 CFU/ml. Each larva was swabbed with 70% ethanol to prevent contamination of the injection site and injected with 10 μL of bacterial dilution using a 50 μL Hamilton syringe. The negative control group was injected with 10 μL of sterile PBS. Then, every five injected larvae were incubated in 10 cm plates at 37 °C, and the number of dead larvae was monitored for the next 48 h. Larvae were scored as dead if they failed to respond to mechanical stimulation of the head. Statistical analysis was performed using the Mantel-Cox test, and *p* values were corrected using the Benjamini–Hochberg method.

Rhamnolipids quantification

Rhamnolipids were extracted from supernatants (2 mL) using ethyl acetate. The extraction was performed twice, and the collected organic fractions were left to evaporate overnight. The resulting white solid precipitates were dissolved in water (100 μL) and mixed with a 0.19% (wt/vol) orcinol solution (900 μL) freshly prepared in 50% H_2SO_4. The samples were heated at 80 °C for 10 min and cooled to room temperature for 10 min before measuring absorbance at 421 nm. Three biological and three technical replicates were performed to ensure experimental reproducibility.

Swarming motility

The swarming motilities of PAO1 WT, Δ*pqsS*, and Δ*pqsS*+ strains were examined by using 0.5% (w/v) agar and 8 g/L nutrient broth supplemented with 0.5% (w/v) glucose. Bacterial culture (1 μL; OD_{600} = 1) was inoculated at the center of the Petri dishes and sat for 30 min, then incubated at 30 °C for 24 h for visualizations. Bacteria spreading from the inoculation spot was measured with a sliding caliper. Three biological and three technical replicates were performed to ensure experimental reproducibility.

Biofilm formation

Biofilm formation was quantified by crystal violet staining. Overnight LB-grown bacterial cultures were diluted in fresh medium (1:100) and incubated in 2 mL of LB in 96-well culture plates at 37 °C for 24 h with 50 rpm allowing stable biofilm formation. After removing the spent media, we removed the loosely associated bacteria by washing them with water two times, and the remaining bacteria were stained with 0.1% crystal violet for 20 min. Then, the crystal violet stain was discarded while the stained biofilms were washed twice thoroughly with ddH_2O and air-dried. The stained biofilm was then dissolved into 200 μL of 95% ethanol and quantified at 630 nm using a Tecan Infinite 200 Pro plate reader.

Confocal microscopy imaging of biofilm

Confocal microscopy imaging of biofilm was adapted from the previous protocol[35]. To visualize bacterial biofilm formation, we cultured overnight grown bacterial cultures in 20 mm glass-bottom culture dishes (Biosharp, China). After 24 h of incubation at 37 °C with 50 rpm allowing stable biofilm formation, the supernatant was removed, and the well surface was rinsed briefly with 0.9% NaCl. One milliliter of 0.9% NaCl containing 1 μM of SYTO 9 (Invitrogen, USA) was added to the well, and the plate was incubated for 15 min in the dark. Fluorescent images were acquired with a confocal microscope (Zeiss LSM 900, German) for monitoring fluorescence and analyzed using the Comstat software. Experiments were performed in triplicate, and representative images are shown. To evaluate the colistin resistance, after 12 h biofilm formations, samples were challenged with 10 μg/mL colistin overnight. Planktonic cultures were then discarded, and the biofilms grown in the plates were washed with sterile PBS once before being stained with the LIVE/DEAD BacLight kit (Invitrogen, USA) for 20 min.Cells stained green with SYTO-9 indicated live cells, while cells stained red with propidium iodide (PI) indicated dead cells.

Macrophage phagocytosis and bacteria survival assay

The method for macrophage intracellular survival assays was adapted from the previous protocol[36]. Mid-log phase bacteria (OD600 = 0.6) grown in LB

broth were centrifuged and resuspended in PBS to infect RAW264.7 macrophages grown in DMEM medium supplemented with 10% FBS at an MOI of 100. After centrifugation of 24-well culture plates, bacterial phagocytosis was allowed to proceed for 30 min before washing three times with sterile PBS and adding fresh DMEM media supplemented with 400 μg/mL gentamicin. After 2 h infection, macrophages were lysed by using 1% Triton X-100 and the number of viable bacteria was determined by subsequent plating onto LB agar plates. The percentage of survival represents the ratio between the number of bacteria at time 2 h and the number of bacteria internalized after phagocytosis.

Cellular ROS production measurement by DCFH-DA staining in flow cytometer

ROS production level in RAW264.7 cells cultured for 2 h after phagocytosis was detected by Reactive Oxygen Species Assay Kit (Beyotime, China). Briefy, RAW264.7 cells were infected with the isolates respectively at a Multiplicity of Infection (MOI) of 100 at 37 °C in 5% CO_2 incubator. After 2 h infection, cells were washed with PBS and incubated with the 2'-7'dichlorofluorescin diacetate (DCFH-DA) (final concentration 10 μM) reagent at 37 °C for 20 min in DMEM medium without FBS. The cells were washed with PBS and harvested. The stained cells were analyzed by using a Cytofex S flow cytometer (Beckman, USA). All samples were assayed with lasers emitting at 488 nm, and the fluorescence was collected by 530/30 nm bandpass filter. The flow cytometric data were analyzed using FlowJo software.

Real-time (RT)-quantitative (q) PCR

Bacterial strains were grown in the LB medium until they reached the mid-exponential phase (OD600 ~ 0.6). Total bacterial RNA was extracted using an EASYspin Plus bacterial microRNA kit (Aidlab, China) and treated with RNase-free DNase I to eliminate genomic DNA contamination. The RNA concentration was measured using a Nanodrop 2000 spectrophotometer (Thermo Fisher). One microgram of the diluted extracted RNA was converted to cDNA using the PrimeScript RT Reagent Kit with gDNA Eraser (Perfect Real Time) (TaKaRa, Japan). Validated primers (Supplementary Table 1) and ChamQ Universal SYBR qPCR Master Mix (Vazyme, China) were added to the cDNA. The mixture was amplified using QuantStudio 1 (Applied Biosystems, USA), and three replicates were obtained. The data were collected using QuantStudio Real-Time PCR software v1.3, normalized to endogenous *rpsL* levels, and analysed using the comparative critical threshold (C_T) method. All reactions were conducted in triplicate. Furthermore, to test the effect of the PqsS sRNA on target gene *pqsL* mRNA stability, the corresponding bacteria were grown to reach an OD_{600} of 1.0, followed by treatment with 100 μg/mL rifampicin. At each indicated time point after rifampicin treatment, the same volume of bacteria was harvested, and the corresponding RNA was extracted immediately for RT-qPCR.

Green fluorescence protein (GFP) reporter gene assay

For the *pqsA* promoter-*gfp* and *pqsS* promoter-*gfp* reporter fusion strains, the corresponding plasmid was introduced into corresponding strains by electroporation. Transformants were selected on LB agar plates containing 100 μg/ml carbenicillin. Overnight cultures (grown in LB medium at 37 °C, shaking at 200 rpm) were diluted in ABTGC medium to an OD_{600nm} of 0.02 (~2.5×10^8 CFU/mL). A blank control (ABTGC medium) was used. The microtiter plate was incubated at 37 °C in a Tecan Infinite 200 Pro plate reader (Tecan Group Ltd., Mannedorf, Switzerland) to measure the cell density (OD_{600nm}) and GFP fluorescence (excitation at 485 nm, emission at 535 nm) at 1 h intervals for 24 h.

LC-MS/MS analysis of PQS, HQNO, and HHQ

1 mL overnight bacteria culture fluid (OD 1.0) was centrifuged at 10,000 × *g* for 10 min, and the supernatant was filtered through a 0.2 μm Millex Syring Filter. Then, the bacterial supernatants were resuspended in an equal volume of methanol and stored at −20 °C. The extract was subjected to LC-MS/MS with a C18 reverse-phase column, as previously reported[37]. Briefly, a C18 reverse-phase column connected to a mass spectrometer was used to separate the hydroxyl-alkyl-quinolones using a water/acetonitrile gradient. Positive electrospray in the MRM mode with 261023 mTorr argon and 30 V as the collision gas were employed to quantify hydroxyl-alkyl-quinolones using the ion transitions HHQ 244.159, HQNO 260.159, PQS 260.175. All MS experiments in this study were performed on a Q Exactive Orbitrap Mass Spectrometers (Thermo Scientific, USA). Analyst software was applied for data acquisition and processing.

Western blotting

To analyze the PqsL protein levels, total proteins were separated by 12% sodium dodecyl sulfate-polyacrylamide and transferred onto polyvinylidene difluoride membranes. The membranes were treated with 5% non-fat milk for 1 h and incubated with the primary antibodies against the FLAG-tag, RNA Polymerase α (α-RNAP), Hfq, or RNase E at 4 °C overnight, followed by washing in tris-buffered saline (TBST). The blots were further incubated with a secondary goat anti-mouse-HRP antibody (Abcam, UK) at room temperature for 1 h. The blots were washed in TBST before detection with enhanced chemiluminescence reagent and an ECL Western Blotting Substrate Kit (Abcam, UK). FIJI/ImageJ software was used to measure band intensities.

RNA-RNA electrophoretic mobility shift assays (REMSA)

DNA templates were transcribed into PqsS (+, negative-strand), PqsS (-, positive-strand, positive control), *pqsL* mRNA, using a T7 High-Efficiency Transcription Kit (TransGen, China). The purified RNA was checked on an 8% Tris-Acr-Urea gel. Then, REMSA was performed with PqsS (+, 0.5, 1, 2, and 4 μM), PqsS (-, positive control, 1 μM), *pqsL* mRNA (1 μM), in 10× REMSA binding buffer. The reaction mixtures were incubated for 2 min at 85 °C and then at 37 °C for 30 min. RNA was separated on an 8% native polyacrylamide gel electrophoresis (PAGE) using a Native-PAGE Preparation kit (Sangon, China), stained with SYBR™ Gold Nucleic Acid Gel Stain (Invitrogen, USA) for 10 min, and visualized under a UV light.

RNase E cleavage assay

N-terminal RNase E (1-529 aa) was purified as described previously[38]. In vitro transcribed *pqsS pqsL*, and *rpsL* DNA templates were generated using a T7 High-Efficiency Transcription kit (TransGen, China). Transcripts of the indicated concentrations were incubated in REMSA binding buffer for 2 min at 85 °C, followed by incubation at 37 °C for 30 min. Then, RNase E was added to a final concentration of 7.5 μM, and the samples were incubated for 30 min at 37 °C. Then, the samples were subjected to electrophoresis on a 1.2% agarose gel containing formaldehyde. After electrophoretic transfer to a Brightstar Plus nylon membrane, the membranes were crosslinked by 85 °C. The specific biotin-labeled primer at an optimized concentration, was added to fresh hybridization buffer, and the blots were incubated in buffer overnight. Then, the signal was detected using the biotin chemiluminescence detection kit (Beyotime, China). Hybridization signals were visualized on an Amersham Imager 680.

Extraction and purification of *P. aeruginosa* membrane vesicles (MVs)

Bacterial strains were grown in TSB until the exponential phase. Bacterial cells were harvested by centrifugation at 8000 × *g*, 4 °C for 15 min. The supernatant was passed through a 500 mL Vacuum bottle with a 0.45 μm filter (Biofil, China) and then concentrated in Masterflex Easy-Load with 100 KD Vivaflow membranes (Sartorius AG, German). The concentrated supernatants were incubated with 2 μg/mL RNase A/T1 (Thermo Scientific) for 1 h at 37 °C before centrifugation at 50,000 × *g* for 2 h at 4 °C to pellet the crude MVs. The MVs were purified by density gradient centrifugation (ranging from 15 to 60%) at 100,000 × *g* with Opti-Prep Gradient Medium (Sigma Aldrich, USA) for 16 h at 4 °C. The 35–45% layer containing purified

MVs were washed in PBS for 1.5 h at 4 °C. Final purified MVs pellets were resuspended in PBS.

Characterization of MVs by Transmission electron microscopy (TEM), and Nanoparticle tracking analysis (NTA)

Purified MVs were visualized by negative staining TEM. In brief, 5 μL of the MVs were incubated for 1 min on a glow-discharged 200-mesh carbon grid (Zhongjingkeyi Technology, China) and contrasted with a phosphotungstic acid solution. Subsequently, the grids were viewed on an HT7700 transmission electron microscope (Hitachi, Japan) operating at 100 kV and fitted with a high-sensitivity real-time charge-coupled device camera. For NTA, the quantification and size characterizations of the MVs were performed on a NanoSight NS300 (Malvern Instruments Ltd, UK). For the size and concentration measurements, a 448 nm laser in scatter mode was used. Briefly, MV samples were diluted (500×) in PBS to obtain a concentration within the recommended measurement range ($1–10 \times 10^8$ particles/mL). Using a 1 mL syringe, the sample was injected into the instrument and videos were captured in triplicate for 30 s. The mean values for size and concentration were analyzed using the NanoSight (NTA software, version 3.0). For northern blotting, we performed a RNase digestion step to remove RNAs outside MVs, samples were incubated with 10 ng/μL RNase A/T1 (Thermo Scientific, USA) for 30 min at 37 °C, diluted 1/100 with water and pelleted at 50,000 × *g* for 1 h to remove the external RNase.

Phylogenetic analysis of *pqsS* and bioinformatics analyses

Public complete genomes from 83 *P. aeruginosa* strains marked as human isolates were downloaded from the *Pseudomonas* genome database (access date 12 August 2021)[39], which were then used to build a nucleotide database with makeblastdb[40]. BLASTn was then used to search the *pqsS* gene against this database. Nucleotide sequences used to construct the phylogenetic tree were aligned using MAFFT, and a maximum-likelihood tree was constructed using PhyML of Unipro Ugene and FigTreev1.4.3 based on the General Time Reversible (GTR) model[41] of nucleotide substitution with c-distributed rates among sites. IntaRNA was used to predict the interaction region between RNAs. Softberry Boot Programmable Read-Only Memory (BPROM) was used to predict bacterial promoters and potential upstream proteins based on transcription factor-binding sites.

Statistical analysis

All statistical analyses were performed using GraphPad Prism software; the data were analyzed by a two-sided Mann–Whitney U test and Benjamini-Hochberg-corrected *P* values. The data represent the means ± SD of three independent experiments unless otherwise indicated. $P < 0.05$ were considered statistically significant. All false discovery rate controls were performed with the Benjamini-Hochberg procedure, and a false discovery rate of 10% ($q < 0.1$) was selected as the significant threshold. Statistical details for all tests performed can be found in the Fig. legends.

Results

The PqsS is an Hfq chaperone-binding sRNA in *P. aeruginosa* PAO1

By analysing publicly available High-throughput Global sRNA target identification by Ligation and sequencing (Hi-GRIL-seq) data of sRNAs from *P. aeruginosa* strain PAO1[42], we screened them by removing known sRNAs and retaining unknown sRNAs with lengths between 200 and 500 nt. The remaining 12 sRNAs are listed in Supplementary Table 2. Among them, a potential sRNA IG_minus_901047_901519 was renamed to PqsS, which is encoded by the intergenic region between the genes *PA0826* and *PA0827* (Fig. 1a). To confirm that PqsS is an sRNA that is transcribed into PAO1, northern blotting was performed using a PqsS-specific probe. The results showed that *pqsS* was transcribed in PAO1 wild-type (WT) and the complementary Δ*pqsS* mutant of this strain (Δ*pqsS*+), but not in the Δ*pqsS* mutant (Fig. 1b). We then introduced a specific promoter-less plasmid (pJV300) containing *pqsS* with its predicted promoter region into the Δ*pqsS* mutant. Northern blotting showed that this plasmid also led to normal expression of PqsS sRNA compared to that observed in PAO1 WT and normal complement strains. These results revealed that PqsS is an sRNA that is independently transcribed from the reverse strand of the genome, with a size of approximately 230–250 nucleotides in PAO1 WT (Fig. 1b). Furthermore, 5' monophosphate-dependent terminator exonuclease (TEX) degrades processed sRNAs while sparing mature sRNAs[43]. The published high-throughput sequencing data for TEX-treated *P. aeruginosa* RNAs[44] also included PqsS, confirming that PqsS is an independently transcribed mature sRNA (Supplementary Fig. 1a).

BPROM online tool analysis suggested a putative unique promoter region for *pqsS* upstream of its TSS. Next, we determined the TSS of *pqsS* by fluorescent primer extension and found that it was identical to that predicted by BPROM analysis (Supplementary Fig. 1b). We then mapped the TSS (+1) of the *pqsS* coding sequence to positions $A_{5,362,926}$ (adenine at 901,479 bp of the forward strand) in the PAO1 genome (6,264,404 bp total)[45] (Fig. 1a). The total size of PqsS was determined to be 239 nt by direct nanopore RNA-seq of *P. aeruginosa* PAO1, which generated long reads for full-length RNAs in an unbiased manner (Supplementary Fig. 1c). The termination site of the *pqsS* coding sequence was mapped to $T_{5,363,165}$ (thymine at 901,240 bp on the forward strand) of the genome (Fig. 1a). Moreover, RT-qPCR results showed that the mRNA levels of the adjacent genes *PA0826*, *PA0827*, and *ssrA* did not change after *pqsS* mutation (Supplementary Fig. 1d), indicating that PqsS functions independently of the adjacent genes without inducing a polar effect. Using the online tool RNAfold, we predicted that the secondary structure of PqsS comprised 5 hairpin loops, 11 internal loops, and 5 bulges (Supplementary Fig. 2a).

The Hfq protein is a major sRNA chaperone that binds to sRNAs and protects them from degradation by cellular nucleosidases[26]. Therefore, we examined the effect of *hfq* deletion on PqsS abundance using northern blotting. The presence of PqsS RNA in WT and Δ*hfq*+ strains, which was absent from the Δ*hfq* strain, indicated that Hfq promoted PqsS abundance (Fig. 1c). We then verified the interaction between PqsS and Hfq using a protein-RNA EMSA with in vitro transcribed PqsS sRNA and purified Hfq protein. EMSA reactions were performed using different concentrations of Hfq protein but a fixed amount of PqsS sRNA. We successfully observed Hfq-PqsS complexes and found that the band intensity increased with increasing Hfq concentration (Fig. 1d), confirming a direct interaction between the Hfq protein and PqsS sRNA in vitro.

We performed a *P. aeruginosa* Hfq hexamer-PqsS sRNA docking analysis to predict the exact interaction sites. Seven PqsS sRNA bases, A40 (adenine, position 40 from the TSS), C42 (cytosine), C113 (cytosine), C116 (cytosine), G134 (guanine), G149 (guanine), and G190 (guanine), appeared to bind to Hfq (Fig. 1a, e). These sRNA bases interacted with four Hfq amino acid residues: Y25 (tyrosine, position 25 from the start codon), G29 (glycine), K31 (lysine), and T49 (threonine) (Supplementary Fig. 2b). Finally, to confirm that the seven nucleotides (A40, C42, C113, C116, G13, G149, and G190) constituted the key sequence of PqsS required for binding to Hfq, we repeated the EMSA using a mutated PqsS ($PqsS^{*\text{-Hfq}}$) sRNA (A40, C42, C113, C116, G13, G149, and G190 were complementary to U40, G42, G113, G116, C13, C149, and C190) generated by in vitro transcription. No interactions were observed between $PqsS^{*\text{-Hfq}}$ sRNA and Hfq proteins (Supplementary Fig. 2c). These results showed that PqsS is an sRNA in *P. aeruginosa* PAO1 that binds to the Hfq chaperone via seven key nucleotides (A40, C42, C113, C116, G13, G149, and G190).

PqsS promotes PAO1-mediated acute infections including host cell death and RL-regulated swarming motility

Growth curves showed that PAO1 WT, Δ*pqsS*, and Δ*pqsS*+ strains grew at similar rates in vitro (Fig. 2a). Therefore, we tested the influence of PqsS on bacterial virulence in vitro and in vivo using macrophage killing and *Galleria mellonella* infection assays, respectively. We leveraged RAW264.7 murine macrophages and A549 human lung epithelial cells as representative cell models of *P. aeruginosa* infection. We infected both cell types with PAO1 WT, Δ*pqsS*, and Δ*pqsS*+ complementary strains and then determined

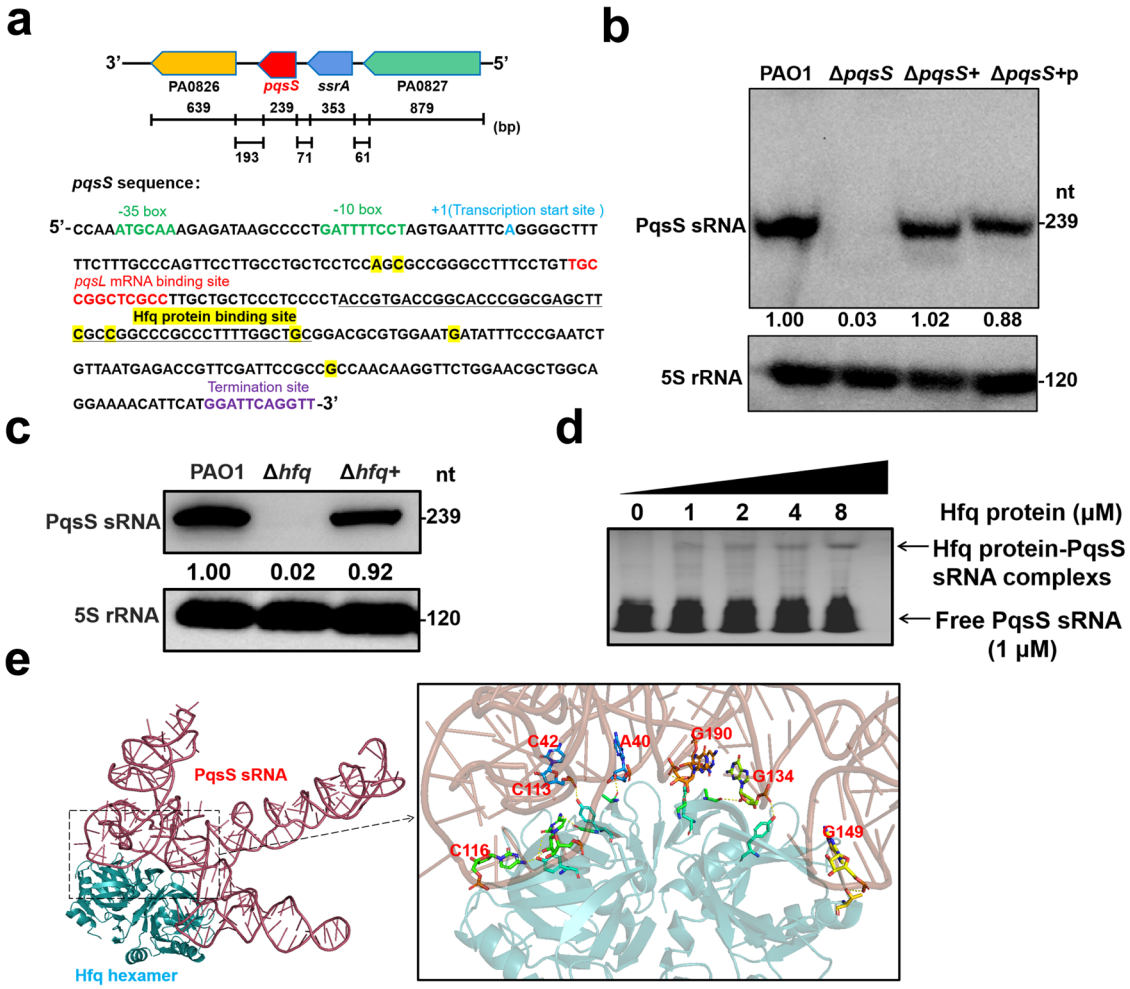

Fig. 1 | Identification and characterization of a novel Hfq hexamer-binding sRNA PqsS in *P. aeruginosa* PAO1. a Upper panel: the position of the *pqsS* in the PAO1 genome between *PA0826* and *PA0827*, yellow box; *PA0826*, red box; *pqsS*, blue box; *ssrA*, green box; *PA0827*. Downward panel: *pqsS* sequences: −35 and −10 boxes of the putative promoter region, green; transcription start site, blue; *pqsL* mRNA binding site, red; Hfq protein binding site, highlighted; and termination site, purple. **b** Northern blotting was performed with a specific probe directed against PqsS sRNA in RNA preparations from PAO1 WT, Δ*pqsS*, and Δ*pqsS* mutant expressing *pqsS* from a rescue construct using the pMiniCTX1-*pqsS* plasmid 's own promoter (Δ*pqsS* +) or a pJV300 plasmid using the *pqsS* promoter (Δ*pqsS* + p) ($n = 3$). 5S rRNA was used as the loading control. Densitometric analysis of the bands was performed with ImageJ. **c** Northern blotting was performed with a specific probe directed against PqsS sRNA in RNA preparations from PAO1 WT, Δ*hfq*, and Δ*hfq*+ strains ($n = 3$). 5S rRNA was used as a loading control. Densitometric analysis of the bands was performed using the ImageJ software. **d** Electrophoretic mobility shift assays (EMSA) with PqsS sRNA in the presence of different concentrations of Hfq protein. **e** Docking analysis of the exact interaction sites in the Hfq hexamer-PqsS sRNA complex. The seven key interaction bases (A40, C42, C113, C116, G134, G149, and G190) of PqsS sRNA are shown in red.

cytosolic lactate dehydrogenase (LDH) release as an indicator of cytotoxicity. We found that RAW264.7 macrophages infected with Δ*pqsS* released 2.13-fold and 1.99-fold less LDH compared to those infected with PAO1 and Δ*pqsS*+ strains, respectively (Fig. 2b). For A549 epithelial cells, we found that the cells infected with Δ*pqsS* released 3.24-fold and 3.09-fold less LDH compared to those infected with PAO1 and Δ*pqsS*+ strains, respectively (Supplementary Fig. 3a). Besides, we performed bacterial adherence assay of PAO1 WT, Δ*pqsS*, and Δ*pqsS*+ strains comparing inocula by plate counts. The results showed that PqsS promoted *P. aeruginosa* adherence to A549 human lung epithelial cells (Supplementary Fig. 3b). In the in vivo *Galleria mellonella* infection model, we found that the Δ*pqsS* strain showed 2.03-fold and 1.97-fold lower mortality compared to PAO1 WT and Δ*pqsS* + strains at 24 h post-infection. The untreated and PBS control samples showed very low mortality rates when used as negative controls (Fig. 2c).

RLs are key virulence factors produced by *P. aeruginosa* that damage the host cells[46]. As expected, RL production by the Δ*pqsS* strain was decreased 1.92-fold and 1.85-fold compared to that of PAO1 and the Δ*pqsS* + strains, respectively (Fig. 2d). Bacterial swarming motility is directly related to RL-mediated acute infection phenotypes. We thus performed a swarming motility assay and found that the growth radii decreased by 1.89-fold and 1.85-fold in the Δ*pqsS* mutant (38 mm) compared to the PAO1 WT (72 mm) and the corresponding complement (71 mm) strains, respectively (Fig. 2e). Taken together, these results suggest that PqsS promotes RL production in *P. aeruginosa*, swarming motility, and macrophage death under in vitro conditions along with the killing of *G. mellonella* under in vivo conditions to enhance acute infections.

PqsS reduces PAO1-mediated chronic infections including biofilm formation, antibiotic resistance, macrophage survival, and reactive oxygen species (ROS) productions

Biofilm formation by *P. aeruginosa* is a well-known cause of chronic infections[47]. The effect of PqsS on biofilm formation was determined using crystal violet staining. The biofilm formation of Δ*pqsS* mutant was increased by 1.59-fold and 1.64-fold, which was comparable to that of the PAO1 WT and Δ*pqsS*+ strains, respectively (Supplementary Fig. 3c). Confocal laser scanning microscopy was used to observe the surface-attached biofilms. Consistent with the results from CV staining, the Δ*pqsS* mutant showed a 1.87-fold and 1.96-fold increase in biomass attached to the surface

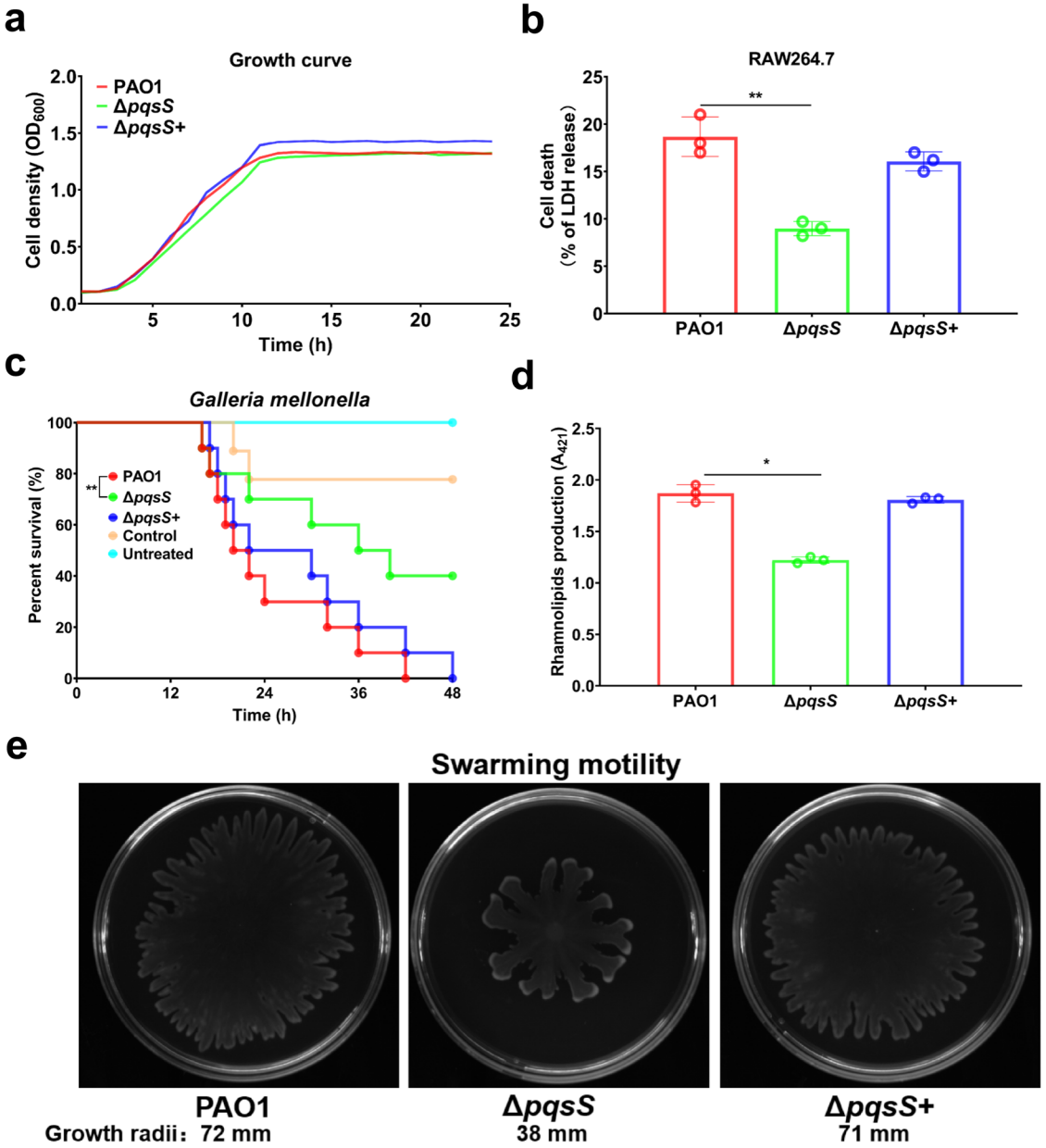

Fig. 2 | PqsS promotes PAO1 acute infections including host cell death and rhamnolipid-regulated swarming motility. a Growth curves of PAO1 WT, Δ*pqsS*, and Δ*pqsS*+ strains. Data represent the means ± standard deviations (SD) ($n = 6$). **b** LDH assay for cell death in RAW 264.7 murine macrophages infected with PAO1 WT, Δ*pqsS*, and Δ*pqsS*+ strains. Data represent the means ± SD ($n = 3$, $^{**}P \le 0.01$, Mann–Whitney *U* test). **c** In vivo measurement of virulence of the PAO1 WT, Δ*pqsS*, and Δ*pqsS*+ strains in a *Galleria mellonella* infection model ($n = 10$, Mantel-Cox test for statistics, $^{**}P \le 0.01$). Each treated group was injected with a 10 μL bacteria dilution, the negative control group was injected with 10 μL sterile PBS, whereas the untreated group was not injected. **d** The production of rhamnolipids by PAO1 WT, Δ*pqsS*, and Δ*pqsS*+ strains ($n = 3$, $^{*}P \le 0.05$, Mann–Whitney *U* test). **e** Swarming motility of PAO1 WT, Δ*pqsS*, and Δ*pqsS*+ strains. All strains were observed after 24 h of growth in 0.5% semisolid medium (8 g/L Nutrition broth, 5 g/L glucose) at 30 °C ($n = 3$).

compared to the WT and Δ*pqsS*+ strains, respectively (Fig. 3a, b). *P. aeruginosa* biofilm formation directly contributes to bacterial antibiotic resistance. Hence, we evaluated how PqsS affected the resistance against colistin, which is a "last-resort" polymyxin antibiotic against multidrug-resistant Gram-negative pathogens[48]. Confocal imaging results showed that the Δ*pqsS* mutant developed 2.37-fold and 2.26-fold increased antibiotic-tolerant subpopulations in response to colistin treatment than the PAO1 WT and Δ*pqsS*+ strains, respectively (Fig. 3c, d).

Chronic infection of *P. aeruginosa* is associated with its ability to resist immune clearance and survive in phagocytic cells[49]. Therefore, we tested whether PqsS affected the phagocytosis rate and intracellular survival of PAO1 in RAW264.7 macrophage infection assay. The *pqsS* mutant behaved similarly to the WT strain with phagocytosis by macrophages (Supplementary Fig. 3d); however, the *pqsS* mutant was less sensitive to macrophage killing than the WT or complemented strains, with a 3.01-fold and 2.95-fold increase in the bacterial survival rate, respectively (Fig. 3e).

Macrophages produce reactive oxygen species, leading to the destruction and clearance of pathogens[50]. Next, we measured the intracellular ROS production in macrophages after infection with PAO1 WT, Δ*pqsS*, and Δ*pqsS*+ strains. We found that the ROS levels within macrophages infected with Δ*pqsS* were 1.91-fold and 1.87-fold lower than those in the PAO1 WT and Δ*pqsS*+ strains, respectively (Fig. 3f, g). These results indicate that PqsS represses *P. aeruginosa* PAO1 chronic infection phenotypes, including biofilm formation, antibiotic resistance, macrophage survival, and ROS production.

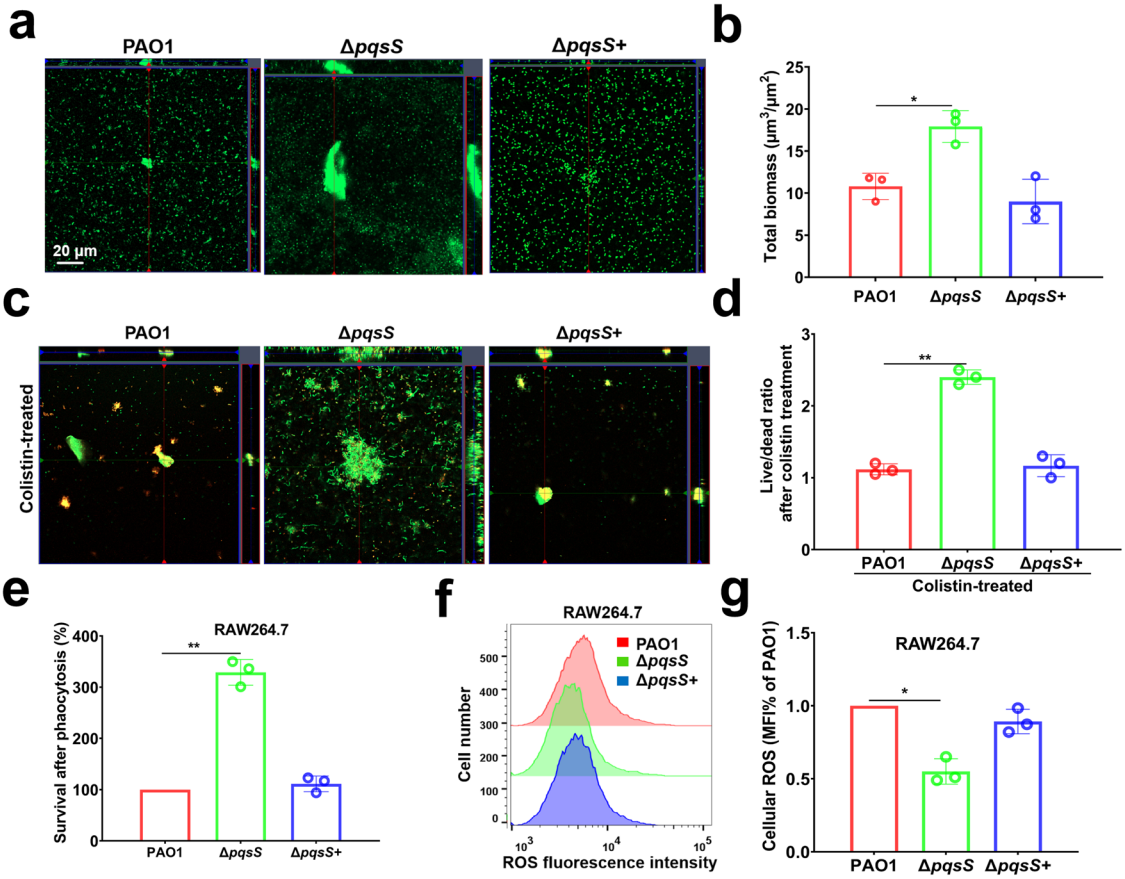

Fig. 3 | PqsS reduces PAO1 chronic infections, including biofilm formation, antibiotic resistance, macrophage survival, and ROS production. a Confocal laser scanning microscopy (CLSM) of biofilms from PAO1 WT, Δ*pqsS*, and Δ*pqsS*+ strains in glass-bottom culture dishes ($n = 3$), scale bar = 20 μm. **b** Biomass were quantitatively analysed using the Comstat software and are expressed as $\mu m^3/\mu m^2$. Data represent the means ± SD ($n = 3$, $^*P \le 0.05$, Mann–Whitney *U* test). **c** CLSM of biofilms after treatment of PAO1 WT, Δ*pqsS*, and Δ*pqsS*+ strains treatment with a medium containing 10 μg/mL colistin ($n = 3$), scale bar = 20 μm. **d** The Live/dead ratio of biofilms after treatment of PAO1 WT, Δ*pqsS*, and Δ*pqsS*+ strains treatment with a medium containing 10 μg/mL colistin. Data represent the means ± SD ($n = 3$, $^{**}P \le 0.01$, Mann–Whitney *U* test). **e** Survival of PAO1 WT, Δ*pqsS*, and Δ*pqsS*+ strains upon phagocytosis by RAW264.7 cells. The results are expressed as the percentage of surviving bacteria compared to the number of bacteria internalized after 2 h after phagocytosis. Data represent the means ± SD ($n = 3$, $^{**}P \le 0.01$, Mann–Whitney *U* test). **f** Flow cytometry for measurement of intracellular reactive oxygen species (ROS) levels in RAW264.7 cells at 2 h after phagocytosis of PAO1 WT, Δ*pqsS*, and Δ*pqsS*+ strains. Data are presented as the means ± SD ($n = 3$). **g** Quantification of intracellular ROS in RAW 264.7 cells treated in (**f**). Data are presented as the means ± SD ($n = 3$, $^*P \le 0.05$, Mann–Whitney *U* test).

PqsS inhibits *pqsL* to increase PQS levels, thereby promoting *pqs* QS system in PAO1

To identify target genes and signaling pathways associated with PqsS, we extracted total RNA (Supplementary Fig. 4a) and performed RNA-seq to detect global gene expression profile differences between the PAO1 WT and Δ*pqsS* strain. In total, 292 genes (130 repressed and 162 activated) were differentially transcribed (>2-fold) between the two strains (Fig. 4a, Supplementary Table 3). Among these, *pqsL*, which encodes a monooxygenase in *P. aeruginosa pqs* QS system, was also predicted by TargetRNA2 as a putative PqsS target (Supplementary Table 4). The results of RT-qPCR analysis were consistent with RNA-seq data, which showed that the *pqsL* mRNA levels increased by 2.1-fold and 2.0-fold in Δ*pqsS* compared to those in PAO1 and Δ*pqsS*+ strains, respectively (Fig. 4b).

P. aeruginosa pqs QS system utilizes the *pqsABCDE* operon and PqsH to synthesise PQS molecules. Specifically, the PQS precursor anthranilic acid was converted by PqsA to produce anthraniloyl-CoA[51], which then formed 2-aminobenzoylacetyl-CoA (2-ABA-CoA) catalyzed by PqsD[52]. This was then converted into 2-ABA by PqsE, formed HHQ by PqsBC[53] and finally converted into PQS by PqsH[54]. Thus, to examine how PqsS sRNAs influence *pqs* QS system, the transcription of *pqsA*, *pqsB*, *pqsC*, *pqsD*, *pqsE*, and *pqsH* was examined via RT-qPCR in PAO1 WT, Δ*pqsS*, and Δ*pqsS*+ strains. The results of RT-qPCR results showed the genes were repressed in Δ*pqsS* strain, which is consistent with our RNA sequencing results (Fig. 4b, Supplementary Table 3). PQS is sensed by its specific receptor PqsR, also known as multiple virulence factor regulator (MvfR), in *P. aeruginosa*[55]. Hence, we knocked out *pqsR* in the negative control. We transformed PAO1 WT, Δ*pqsS*, Δ*pqsS* + , Δ*pqsL*, Δ*pqsL*Δ*pqsS*, and Δ*pqsR* strains with the $P_{pqsA-gfp}$ reporter plasmid[14] to construct PAO1 *pqs* QS system bioreporter strains. Here, the *pqsA* gene expression was monitored to determine the activity of the PAO1 *pqs* QS system[56]. Growth curves showed that PAO1-*pqsA-gfp*, Δ*pqsS*-*pqsA-gfp*, Δ*pqsS* + -*pqsA-gfp*, Δ*pqsL*-*pqsA-gfp*, Δ*pqsL*Δ*pqsS*-*pqsA-gfp*, and Δ*pqsR*-*pqsA-gfp* strains grew at similar rates in vitro (Supplementary Fig. 4b). Using PAO1 $P_{pqsA-gfp}$ and Δ*pqsR* $P_{pqsA-gfp}$ as positive and negative controls, respectively, we found that the expression of *pqsA-gfp* was decreased in Δ*pqsS* $P_{pqsA-gfp}$ compared to that in PAO1 $P_{pqsA-gfp}$ and Δ*pqsS*+ $P_{pqsA-gfp}$ strains. Interestingly, *pqsA-gfp* expression in the Δ*pqsL*Δ*pqsS* $P_{pqsA-gfp}$ strain was similar to that in Δ*pqsL* $P_{pqsA-gfp}$ strain, which itself was higher than that in Δ*pqsS* $P_{pqsA-gfp}$ strain (Fig. 4c). These results suggested that PqsS activated the *P. aeruginosa* PAO1 *pqs* QS system by repressing *pqsL*.

Growth curves showed that PAO1 WT, Δ*pqsL*, Δ*pqsL*Δ*pqsS*, and Δ*pqsR* strains grew at similar rates in vitro (Supplementary Fig. 4c). Monooxygenase PqsL is responsible for converting precursor 2-ABA into

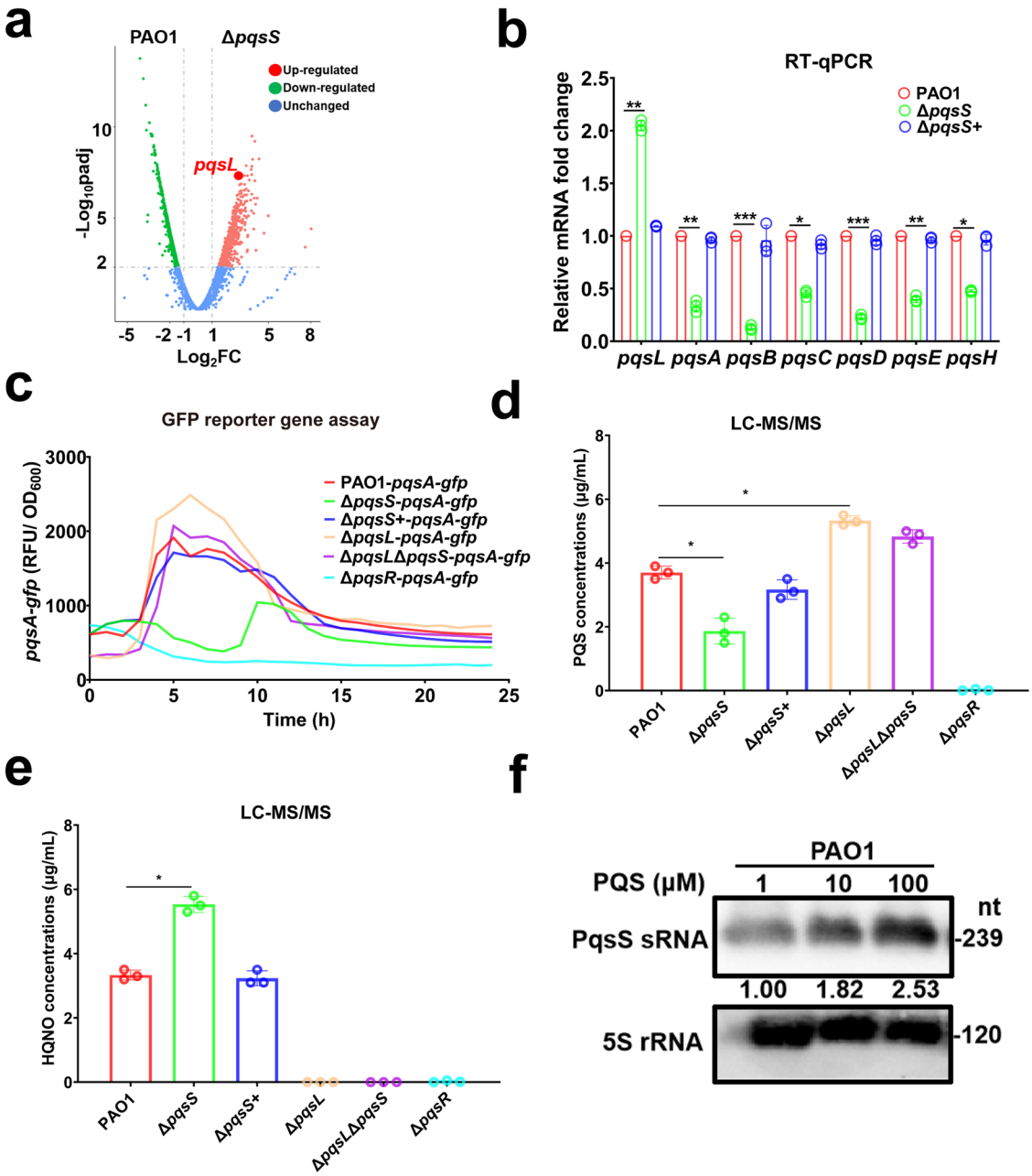

Fig. 4 | PqsS inhibits *pqsL* to increase the amount of PQS for promoting *pqs* QS in PAO1. **a** A volcano plot of the differentially expressed genes (DEGs) determined for PAO1 WT and Δ*pqsS* strains by RNA-seq. FC, fold change; padj, adjusted *p* value. **b** Relative quantification of *pqsL*, *pqsA*, *pqsB*, *pqsC*, *pqsD*, *pqsE*, and *pqsH* expression in PAO1 WT, Δ*pqsS*, and Δ*pqsS*+ strains determined by RT-qPCR. The data are presented as the relative transcript abundance of the indicated genes compared to the internal control transcript for *rpsL* using the comparative Ct method ($2^{-\Delta\Delta CT}$). Data represent the means ± SD ($n = 3$, $^*P \le 0.05$, $^{**}P \le 0.01$, and $^{***}P \le 0.001$, Mann–Whitney *U* test). **c** Expression of $P_{pqsA-gfp}$ reporter fusions in PAO1 WT, Δ*pqsS*, Δ*pqsS* + , Δ*pqsL*, Δ*pqsL*Δ*pqsS*, and Δ*pqsR* strains. The relative fluorescence intensity (reflected as GFP/OD_{600}) was measured in representative strains containing $P_{pqsA-gfp}$ ($n = 3$). **d** Qualification of PQS concentrations measured in the supernatants of PAO1 WT, Δ*pqsS*, Δ*pqsS* + , Δ*pqsL*, Δ*pqsL*Δ*pqsS*, and Δ*pqsR* cultures. Data represent the means ± SD ($n = 3$, $^*P \le 0.05$, Mann–Whitney *U* test). **e** Qualification of HQNO concentrations measured in the supernatants of PAO1 WT, Δ*pqsS*, Δ*pqsS* + , Δ*pqsL*, Δ*pqsL*Δ*pqsS*, and Δ*pqsR* cultures. Data represent the means ± SD ($n = 3$, $^*P \le 0.05$, Mann–Whitney *U* test). **f** Northern blotting analysis of PqsS in PAO1 WT after treatment with the medium containing exogenous 1, 10, or 100 μM PQS for 1 h. 5S rRNA was used as the loading control. Densitometric analysis of the bands was performed using the ImageJ software.

HQNO via a PQS-branched pathway[10]. Hence, we performed LC-MS/MS to measure the production of PQS, the PQS derivative HQNO, and the PQS precursor HHQ. As expected, the Δ*pqsS* mutant produced 1.9 μg/mL of PQS, which was lower compared to 3.8 μg/mL and 3.6 μg/mL observed in PAO1 WT and Δ*pqsS*+ strains, respectively, while Δ*pqsL* (5.5 μg/mL) and Δ*pqsL*Δ*PqsS* (5.3 μg/mL) strains produced more PQS to similar degrees. The Δ*pqsR* strain produced virtually no PQS, as expected in negative control (Fig. 4d). For HQNO, Δ*pqsS* produced more HQNO of 5.7 μg/mL compared to 3.6 μg/mL and 3.5 μg/mL in PAO1 WT and Δ*pqsS*+ strains, respectively. However, Δ*pqsL*, Δ*pqsL*Δ*PqsS*, and Δ*pqsR* strains produced no HQNO (Fig. 4e). HHQ exhibited the same trend as PQS (Supplementary Fig. 4d). Thus, PqsS increases PQS and HHQ production, while decreasing HQNO levels, primarily by inhibiting *pqsL*.

The PQS concentration of normal *P. aeruginosa* secreted in liquid cultures fluctuated from approximately 1 to 60 μM[12,57,58]. To assess whether different PQS concentrations affected PqsS expression, after stimulation

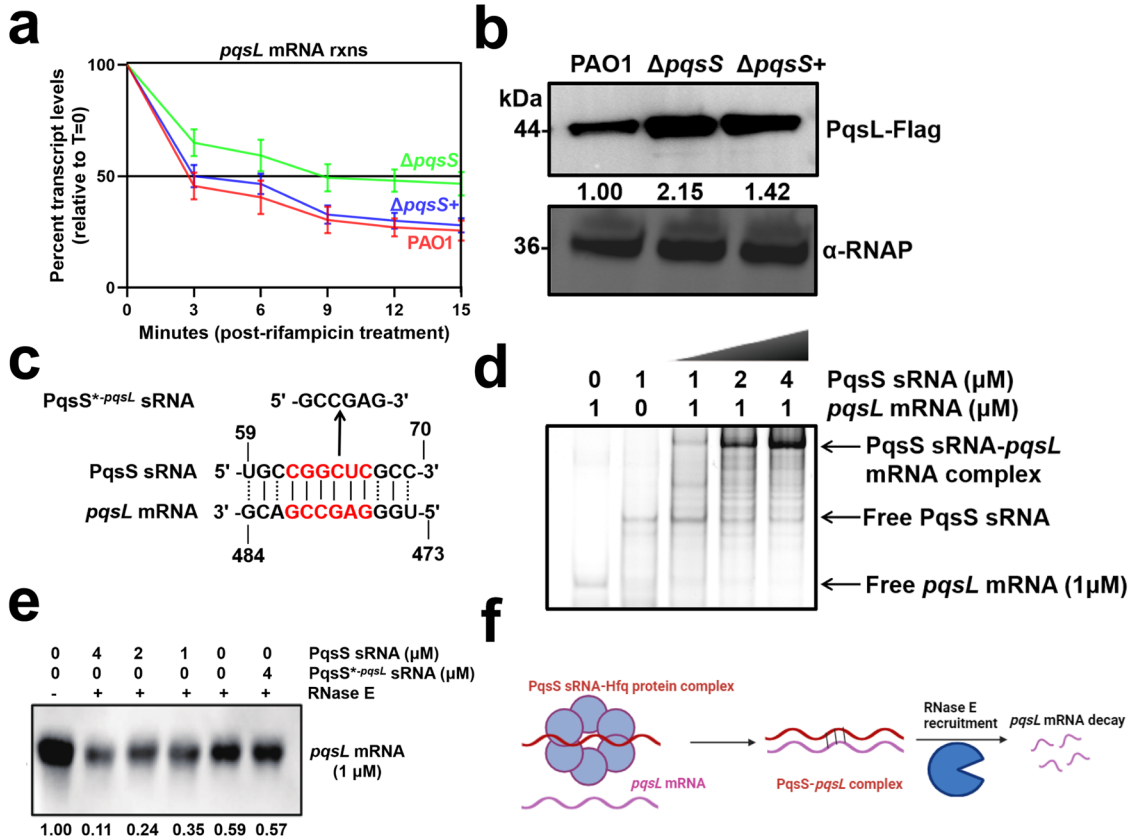

Fig. 5 | Molecular mechanisms of PqsS repressing *pqsL* mRNA stability by triggering RNase E-mediated degradation. a Relative quantification of *pqsL* mRNA by RT-qPCR in rifampicin-treated PAO1 WT, Δ*pqsS*, and Δ*pqsS* + strains for 0–15 min. Data represent the percentage of *pqsL* transcripts relative to time point zero. Data represent the means ± SD ($n = 3$). **b** Representative western blot analysis of PqsL in protein preparations from PAO1 WT, Δ*pqsS*, and Δ*pqsS* + strains. RNA Polymerase α (α-RNAP) served as a loading control ($n = 3$). Protein size (kDa) is indicated on the right side. Densitometric analyses of the bands were performed using the ImageJ software. **c** Predicted base pairing between PqsS sRNA and *pqsL* mRNA. Red letters indicate the predicted binding motif with perfect base pairing. In the in vitro transcribed PqsS$^{*\text{-}pqsL}$ sRNA, the CGGCUC motif was mutated to GCCGAG. **d** REMSA with a fixed amount of *pqsL* mRNA and an increasing amount of PqsS sRNA. **e** In vitro cleavage of *pqsL* mRNA by RNase E in the absence or presence of PqsS sRNA ($n = 3$). Densitometric analyses of the bands were performed using the ImageJ software. **f** Proposed molecular mechanism model of PqsS sRNA inducing *pqsL* mRNA decay by recruiting RNase E.

with exogenous PQS, northern blotting showed that the abundance of PAO1 WT PqsS sRNA was increased by 1.82-fold and 2.53-fold in 10 μM and 100 μM PQS TSB than that in 1 μM PQS TSB, respectively (Fig. 4f). These results confirmed that PqsS represses *pqsL* to stimulate *pqs* QS systems and increase PQS production in *P. aeruginosa* PAO1, whereas high concentrations of PQS further promote PqsS expression, thus forming a positive feedback loop.

PqsS binds to the *pqsL* mRNA to decrease its stability with RNase E cleavage

The antibiotic rifampicin targets bacterial RNA polymerase and is frequently used to inhibit bacterial RNA synthesis and suspend transcription[59]. Researchers have used rifampicin to evaluate the inhibitory effect of sRNA on target mRNA stability at the post-transcriptional level, termed the rifampicin transcription inhibition assay[60]. To determine the exact molecular mechanism by which PqsS represses *pqsL* mRNA, we tested mRNA stability using a rifampicin transcription inhibition assay. Here, *pqsL* mRNA was degraded much more slowly in Δ*pqsS* (half-life: 9.1 min) than in WT (3.2 min) and Δ*pqsS* + (3.3 min) strains, respectively (Fig. 5a). The mRNA stability assay revealed that PqsS sRNA decreased *pqsL* mRNA stability at the post-transcriptional level, further reducing *pqsL* mRNA levels. We then used western blotting to measure the amounts of FLAG-tagged PqsL (PqsL-FLAG) in PAO1, Δ*pqsS*, and Δ*pqsS*+ strains. The *pqsS* deletion increased PqsL-FLAG production by 2.15-fold, and complementation with *pqsS* in Δ*pqsS* restored PqsL-FLAG production (Fig. 5b). Thus, PqsS appears to reduce PqsL production by decreasing the stability of *pqsL* mRNA.

Next, we predicted the complementary 12-nucleotide regions that could mediate the interaction between PqsS sRNA (UGCCGGCUCGCC) and *pqsL* mRNA (UGGGAGCCGACG) using IntaRNA with a six-nucleotide binding motif (CCGCUC) input for PqsS sRNA (Figs. 1a, 5c). The *pqsL* mRNA-binding region was observed in the predicted PqsS sRNA secondary structure (Supplementary Fig. 2a). To test for a direct interaction between PqsS and *pqsL* mRNA in vitro, we performed RNA-RNA EMSA (REMSA) using in vitro transcribed PqsS and *pqsL* mRNA. REMSA reactions were performed using different concentrations of PqsS and a fixed amount of *pqsL* mRNA. We observed the PqsS-*pqsL* mRNA complex with the band intensity appearing enhanced with increasing PqsS concentrations. These findings confirm the direct interaction between PqsS sRNA and *pqsL* mRNA in vitro (Fig. 5d). To confirm that the 6-nucleotide motif (CCGCUC) was the PqsS sequence required for *pqsL* mRNA binding, we performed REMSA using a mutated PqsS (PqsS$^{*\text{-}pqsL}$) sRNA (the motif CCGCUC was mutated to GCCGAG) generated by in vitro transcription. No interaction was observed between PqsS$^{*\text{-}pqsL}$ sRNA and *pqsL* mRNA (Supplementary Fig. 4e), indicating that the PqsS CCGCUC motif was critical for PqsS binding to *pqsL* mRNA.

After discovering that PqsS sRNA decreased *pqsL* mRNA stability, we aimed to explore the underlying mechanism. The best previous example of one bacterial sRNA that binds to target mRNA coding sequence (CDS) and inhibits its mRNA stability is MicC[61]. Specifically, MicC inhibits *ompD* mRNA by binding to its CDS and recruiting RNase E for degradation. RNase E is the most important bacterial RNase for degrading mRNAs[62]; thus, we hypothesized that PqsS reduces the stability of *pqsL* mRNA CDS by

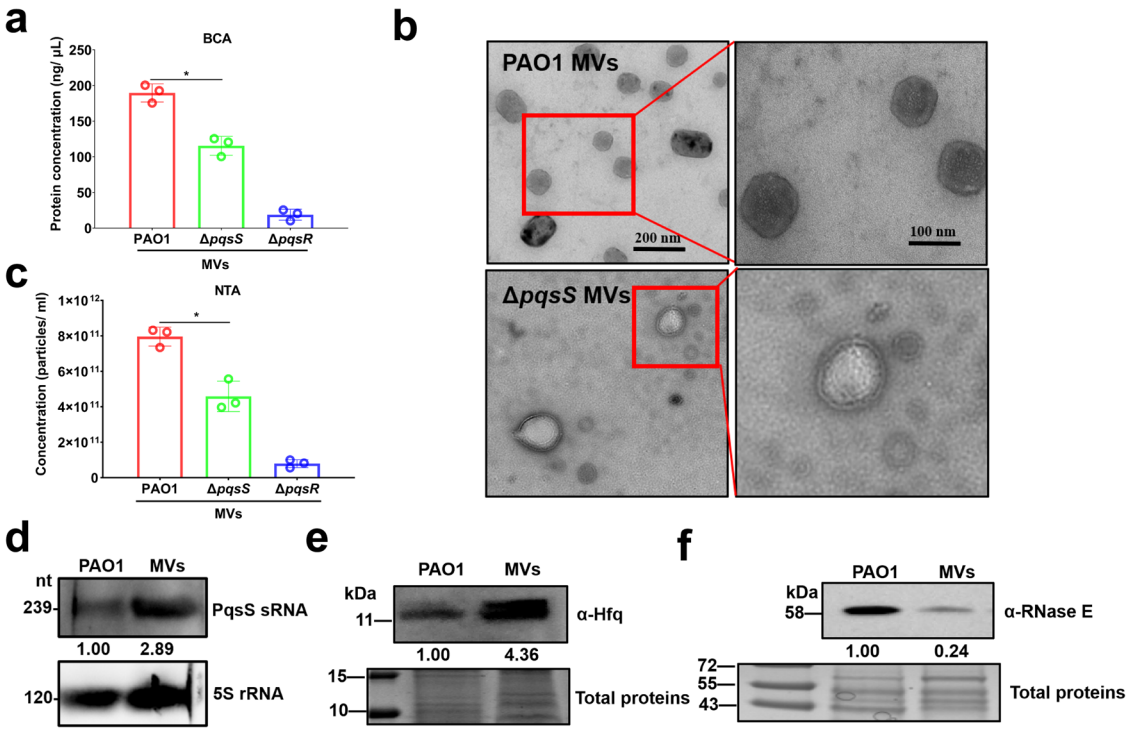

Fig. 6 | PqsS promotes PAO1 MV productions and is abundantly detected in MVs. a Identification of protein content of MVs in PAO1 WT, Δ*pqsS*, and Δ*pqsR* strains via BCA. Data represent the means ± SD ($n = 3$, $^*P \le 0.05$, Mann–Whitney *U* test). **b** Negative staining transmission electron microscopy (TEM) identification of MVs in PAO1 WT and Δ*pqsS* strains ($n = 3$). Scale bar = 200/100 nm. **c** NTA of MV concentrations in PAO1 WT, Δ*pqsS*, and Δ*pqsR* strains. Data represent the means ± SD ($n = 3$, $^*P \le 0.05$, Mann–Whitney *U* test). **d** Northern blotting analysis of PqsS from PAO1 WT and its purified MVs samples ($n = 3$). 5S rRNA was used as the loading control. Densitometric analysis of the bands was performed using the ImageJ software. **e** Western blot analysis of Hfq in protein preparations from PAO1 WT and MVs samples. Total protein served as a loading control ($n = 3$). Densitometric analyses of the bands were performed using the ImageJ software. **f** Western blot analysis of RNase E in protein preparations of PAO1 WT and MVs samples. Total protein served as a loading control ($n = 3$). Densitometric analyses of the bands were performed using the ImageJ software.

facilitating RNase E-mediated cleavage. We performed in vitro RNase E cleavage assays and found that incubation with purified RNase E led to the degradation of the *pqsL* mRNA CDS. Moreover, the addition of PqsS sRNA increased the degradation of *pqsL* mRNA CDS by RNase E (Fig. 5e). However, we did not observe any additional degradation of *pqsL* mRNA CDS upon the addition of $PqsS^{*\text{-}pqsL}$ sRNA. PqsS sRNA did not exhibit any additional degradation effect on the *rpsL* mRNA internal control upon the addition of RNase E (Supplementary Fig. 4f). Thus, we demonstrated the molecular mechanism underlying the interactions of PqsS sRNA-Hfq protein-*pqsL* mRNA-RNase E in which the Hfq-PqsS complex decreased *pqsL* mRNA stability by recruiting RNase E to drive degradation (Fig. 5f).

PqsS promotes PAO1 MVs productions and abundantly detected in MVs

Given that PQS contributes significantly to the majority of planktonic MV formation in *P. aeruginosa*[19], we next investigated whether PqsS sRNA also contributes to *P. aeruginosa* MV production. We performed an optimized *P. aeruginosa* PAO1 MV purification procedure to obtain pure MV without flagella, pili, or Pf4 phage contamination (Supplementary Fig. 5). After MV purification, protein quantification by BCA demonstrated that the total protein amount was reduced by 39% in MVs from the Δ*pqsS* mutant (111.3 ng/μL) compared to those from the PAO1 WT (182.5 ng/μL). Δ*pqsR* mutant (10.9 ng/μL) was used as the negative control (Fig. 6a). The negative staining transmission electron microscopy results clearly showed that the numbers of MVs decreased in Δ*pqsS* mutant compared to those in the PAO1 WT strain. They were nearly 100–200 nm in size and were spherical structures harboring membrane bilayers (Supplementary Fig. 6a). The nanoparticle tracking analyses (NTA) were used to further quantify the number of MVs, which decreased from 7.8×10^{11} particles/mL in PAO1 WT to 4.2×10^{11} particles/mL in Δ*pqsS* mutant. In contrast, Δ*pqsR* mutant (5.6×10^{10} particles/mL) was used as the negative control with nearly unchanged size distributions (Fig. 6c, Supplementary Fig. 6b).

We also performed northern blotting to determine whether PqsS could be detected in the PAO1 MVs. PqsS abundance in MVs was 2.89-fold higher than that in PAO1 WT within the same amount of total RNA extract (Fig. 6d). In addition, the key bacterial sRNA-binding protein Hfq could help sRNAs pack into MVs[63]. Specifically, the C-terminal regions (CTR) of Hfq form amyloid-like structures with fibrils that disrupt bacterial membranes, allowing Hfq to be translocated into the periplasm and exported into MVs[64]. Western blotting was performed to measure the amount of Hfq protein in PAO1 cells and MVs. Hfq protein abundance increased by 4.36-fold in MVs compared to that in PAO1 WT within the same amount of total protein extract. This result indicates that Hfq might ensure sRNA stability in MVs (Fig. 6e). A recently published proteome also showed that RNase E protein levels were decreased by 7.9-fold in MVs compared to those in their parent bacteria[65], which implied that sRNAs are less likely to be degraded by RNase E in MVs. Next, western blotting was used to measure the amount of RNase E in PAO1 cells and MVs. The abundance of RNase E protein decreased by 4.17-fold in MVs compared to that in PAO1 WT within the same amount of total protein extract (Fig. 6f). These results revealed that PqsS sRNA and Hfq protein were abundant in the MVs. Moreover, MVs may protect sRNAs from RNase E.

In addition, we performed comparative genomic analysis to investigate whether *pqsS* is present in other pathogenic *P. aeruginosa* strains. Genome alignment analysis of 83 representative *P. aeruginosa* strains revealed that *pqsS* was highly conserved and widely distributed in 59 strains (59/83) (Supplementary Fig. 7a, b and Supplementary Table 5); however, *pqsS* was not present in other non-*P. aeruginosa* isolates from the *Pseudomonas* genus

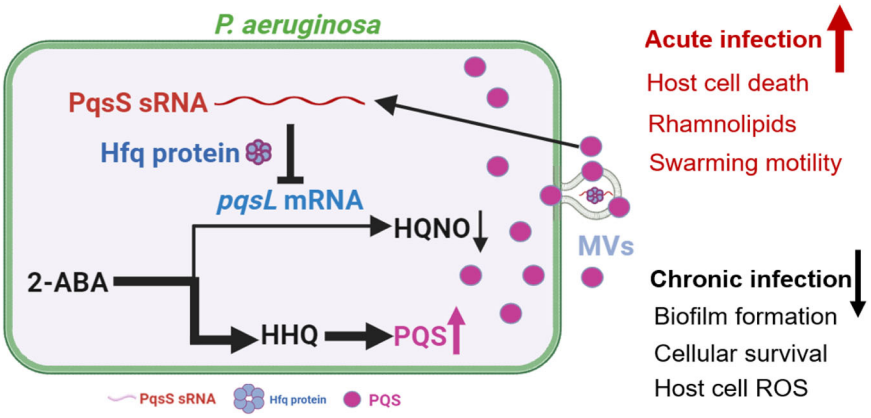

Fig. 7 | Model of the PqsS sRNA-PQS positive feedback to regulate *P. aeruginosa* virulence. A novel sRNA named PqsS promotes *pqs* quorum sensing (QS) with the assistance of the chaperone protein Hfq. Specifically, high levels of PQS promotes PqsS expression and forms a PqsS-Hfq complex. Then, this complex decreases *pqsL* mRNA stability by recruiting RNase E to drive degradation, thereby enhancing PQS productions for *pqs* QS and MVs formation. PQS further promotes PqsS expression, thus forming a positive PqsS-PQS feedback loop. Therefore, PqsS promotes acute bacterial infections including host cell death, rhamnolipids production, and swarming motility, while reducing chronic infections, such as biofilm formation, cellular survival, and host cell ROS production.

(0/117). To investigate whether homologous PqsS in other *P. aeruginosa* strains also suppressed *pqsL* mRNA levels, we knocked down the *pqsS* homolog in *P. aeruginosa* PA14 and quantified the *pqsL* mRNA levels by RT-qPCR. The mRNA level in the mutant was increased by 1.7-fold compared to that in the corresponding WT strain (Supplementary Fig. 7c), implying that PqsS-mediated *pqsL* regulation is conserved in other *P. aeruginosa* strains. Moreover, analysis of publicly available clinical RNA-seq data from *P. aeruginosa* samples showed that the transcription of *pqsS* was increased in human sputum samples[66,67] and SARS-CoV2 infected samples (patients investigated were diagnosed with a secondary *P. aeruginosa* infection)[68] compared to the bacterial liquid culture control (Supplementary Table 6). These results reveal that *pqsS* is conserved in pathogenic *P. aeruginosa* strains and is clinically relevant.

Discussion

P. aeruginosa employs various QS systems to coordinate group behavior and optimize the expression of various regulatory proteins and Hfq-binding sRNAs[69]. In the present study, we explored the potential relationship between Hfq-binding sRNAs and *pqs* QS systems in *P. aeruginosa*. We found that a novel Hfq-binding sRNA-mediated mechanism enabled *P. aeruginosa* to promote *pqs* QS and mediate acute infections (Fig. 7). We first identified PqsS as an Hfq-binding sRNA in PAO1 (Fig. 1). PqsS promoted *P. aeruginosa* acute infections in a macrophage model in vitro and *G. mellonella* in vivo and enhanced RL-mediated swarming motility (Fig. 2). PqsS decreased *P. aeruginosa* biofilm-related chronic infection traits including macrophage survival and ROS production (Fig. 3). Furthermore, we identified *pqsL* as a target gene of PqsS and found that PqsS increased PQS production in an enhanced *pqs* QS system. PQS further promotes PqsS expression, thus forming a positive PqsS-PQS feedback loop (Fig. 4). We also showed that the PqsS-Hfq complex inhibited *pqsL* mRNA by binding to its CDS and recruiting RNase E for degradation (Fig. 5). Finally, PqsS promoted PAO1 MV production and was abundantly detected in the MVs (Fig. 6). These findings highlight an extra sRNA-centered QS signal amplification strategy in *P. aeruginosa* communities, in addition to traditional bacterial QS communication. PqsS enhances *P. aeruginosa* infection. Hence, it may be a potential drug target for the development of anti-*P. aeruginosa* therapy.

P. aeruginosa expresses various sRNAs under specific microenvironmental conditions, such as different ion, oxygen, and metabolite concentrations, to regulate acute or chronic infection mechanisms. Acute infection mechanisms of *P. aeruginosa* include host cell death, virulence factor synthesis, flagella or pili-mediated motility, and T3SS, whereas chronic infection mechanisms include biofilm formation, antibiotic tolerance, and reduced sensitivity to phagocytes[70]. The classification of *P. aeruginosa* sRNAs based on acute and chronic infection regulation is not currently clear; thus, we summarized the previously studied sRNAs into three groups: 1. sRNA can simultaneously promote or inhibit acute and chronic infections simultaneously (eg, ErsA increases motility-related acute infections and biofilm formation-related chronic infections under low oxygen levels[71]); 2. sRNA promote acute and reduced chronic infections (e.g., PrrF1/2 promotes acute bacterial lung infection while reducing biofilm-related chronic infections in response to low-iron conditions[29,72]); 3. sRNA promote chronic infections and reduce acute infections (e.g., RsmY/Z promotes biofilm formation to allow bacteria to adopt a sessile lifestyle, mediating chronic infection under conditions involving high c-di-GMP levels[73,74] while reducing the expression of type IV pili and flagella to downregulate acute infection[70,75]). In this study, we report a novel sRNA, PqsS, which enabled *P. aeruginosa* to promote *pqs* QS, favor acute infections, and repress chronic infections by sensing high PQS concentrations (Fig. 7). Based on our classification method, PqsS belongs to the type two sRNA, which promotes acute infections and reduces chronic infections, similar to PrrF1/2[29,72]. Hence, it may serve as the biomarker for *P. aeruginosa* acute infections. Our novel findings and those of previous sRNA-related studies highlight that bacteria employ multiple sRNAs to control their acute or chronic infections in response to different microenvironmental cues.

To date, multiple molecular mechanisms have been discovered by which bacterial sRNAs downregulate target mRNAs[76–78], including the following: 1. sRNAs pair with the ribosome binding site, a Shine-Dalgarno (SD) sequence, within the 5' untranslated region (UTR) of the target gene to prevent the translation initiation of its protein (eg, PrrF1/2 repressed *antR* mRNA translation by binding to its 5' UTR region[79]); 2. sRNAs pair with the CDS region of the target mRNA, resulting in the degradation of the target mRNA by recruiting RNases and shortening the half-life of the target mRNA to induce mRNA decay (e.g., MicC inhibits *ompD* mRNA by binding to its CDS and recruiting RNase E for degradation[61]); 3. sRNAs cannot change the mRNA quantity but modify the conformation of the mRNA of the target gene such that the gene cannot be expressed normally (e.g., SR1 inhibits *ahrC* translation by inducing structural changes downstream of the RBS site[80]). In our study, we first predicted the interaction region between PqsS sRNA and *pqsL* mRNA within the CDS region (484-473) of *pqsL* mRNA; thus, the inhibitory mechanism cannot be type 1. We tested the influence of PqsS sRNA on *pqsL* mRNA levels using qRT-PCR (Fig. 4b). The results showed that sRNA PqsS decreased the expression level of *pqsL* mRNA; thus, we did not consider type 3. Therefore, we examined the type 2 mechanism by measuring the influence of PqsS sRNA on *pqsL* mRNA stability to determine whether PqsS sRNA mediated transcript decay. Our mRNA stability results revealed that PqsS sRNA decreased *pqsL* mRNA stability at the post-transcriptional level, further reducing *pqsL* mRNA levels (Fig. 5a). We also found that PqsS sRNA increased *pqsL* mRNA CDS degradation by RNase E (Fig. 5e). Thus, we elucidated the molecular mechanism underlying the induction of *pqsL* mRNA decay via the recruitment of RNase E by PqsS sRNA (Fig. 5f).

Many *P. aeruginosa* sRNAs have been studied for their roles in biofilm formation. However, most previous studies have focused on the regulatory

effects of sRNAs inside bacteria. These regulatory effects on biofilm formations are indirect. For example, the expression of SicX small interfering RNA (sRNA) is induced under low oxygen levels to promote chronic biofilm formation[81]. Recently, extracellular RNAs (eRNAs), whose spatial position is closer to the actual biofilm structure than that of endobacterial RNAs, has garnered significant interest. Substantial amounts of eRNAs such as *ssrA* and *crcZ* can be detected within biofilms, contributing to their structural integrity and viscosity within biofilms[82]. However, a stable eRNA source in the biofilm matrix remains elusive due to the natural instability of RNA molecules. MVs are essential components of *P. aeruginosa* biofilms[18,83,84]. Another recent study showed that the total RNAs of MVs contained 60% short RNA fragments[85]. We hypothesized that small regulatory eRNAs may also contribute directly to biofilm matrix formation (*i.e.* as biofilm matrix components). Thus, MVs may be a valuable source for identifying novel bacterial sRNAs and revealing their functions in biofilm regulation. Our study revealed that a specific sRNA, PqsS, was abundantly detected in MVs and decreased biofilm formation (Figs. 3a, b, and 6d). However, the total eRNA promotes biofilm formation[82]. Hence, we propose that this is due to a dynamic homeostasis in biofilm formation, indicating that not all sRNAs facilitate biofilm formation. Under a specific microenvironment, bacteria express chronic infection-regulated sRNA, such as SicX, to prefer a biofilm lifestyle, whereas when the condition changes, *P. aeruginosa* may utilize sRNAs, such as acute infection-regulated PqsS, to switch to a planktonic lifestyle.

Bacterial MVs can fuse with nearby membrane-structured organisms to exchange cargo, thereby playing an important role in inter-cellular communication[83]. MVs can carry various hydrophobic molecules, proteins, and nucleic acids that travel long distances and target other bacteria for nutrient acquisition. For example, TseF, a *P. aeruginosa* T6SS effector incorporated into MVs, directs MVs to their parent bacteria by binding to the surface receptors, FptA and OprF, to acquire MV-associated iron[86]. In addition, MVs may interfere with other bacteria in nearby ecological niches, thus helping bacterial cells compete for nutrients in a limited environment[87]. For instance, *P. aeruginosa* MVs contain a high level of hydrophobic PQS signaling molecules[88], which can travel a long distance (cm scale, much longer than the normal QS diffusion distance) at the solid surface to eradicate *S. aureus* colonies[89]. Despite multiple studies investigating the virulence factors encapsulated in *P. aeruginosa* MVs, the potential intercellular regulatory roles of MV-carried RNA components remain largely unknown and warrant further investigation.

Comparative genomics analysis showed that PqsS also exists in various clinical *P. aeruginosa*-infected samples (Supplementary Table 6). Thus, determining the exact host cell targets and the regulatory network of PqsS during infection requires further investigation. Bacterial MV-enriched sRNAs have been reported to modulate host cell functions. In *P. aeruginosa*, MV-enriched sRNA-sRNA52320 (a 23-nt tRNA fragment) attenuated interleukin-8 secretion in human airway epithelial cells[90]. Other bacteria also use MV-enriched sRNAs to modulate host-microbe interactions. For example, *E. coli* sRNA Ile-tRF-5X is released via MVs and promotes human HCT116 cell MAP3K4 expression[91]. In another study, *Legionella pneumophila* MVs translocated the sRNA RsmY into host cells and mimicked eukaryotic microRNAs to reduce host defense signaling pathways[92]. The results of our study, together with previous findings, enrich our understanding of the fascinating world of sRNAs and their intricate roles in bacterial pathogenesis.

Reporting summary

Further information on research design is available in the Nature Research Reporting Summary linked to this article.

Data availability

RNA-seq data have been deposited into the Sequence Read Archive database (https://www.ncbi.nlm.nih.gov/sra) with the bioProject accession number: PRJNA982285 (Nanopore PAO1 RNA-seq), PRJNA916110 (Δ*pqsS* RNA-seq).

Received: 3 April 2024; Accepted: 20 August 2024;
Published online: 11 September 2024

References

1. Curran, C. S., Bolig, T. & Torabi-Parizi, P. Mechanisms and targeted therapies for pseudomonas aeruginosa lung infection. *Am. J. Respir. Crit. Care Med.* **197**, 708–727 (2018).
2. Rice, L. B. Federal funding for the study of antimicrobial resistance in nosocomial pathogens: no ESKAPE. *J. Infect. Dis.* **197**, 1079–1081 (2008).
3. Ciofu, O., Moser, C., Jensen, P. & Høiby, N. Tolerance and resistance of microbial biofilms. *Nat. Rev. Microbiol.* **20**, 621–635 (2022).
4. Lichtenberg, M. et al. The structure-function relationship of Pseudomonas aeruginosa in infections and its influence on the microenvironment. *FEMS Microbiol. Rev.* **46**. https://doi.org/10.1093/femsre/fuac018 (2022).
5. Balasubramanian, D., Schneper, L., Kumari, H. & Mathee, K. A dynamic and intricate regulatory network determines Pseudomonas aeruginosa virulence. *Nucleic Acids Res.* **41**, 1–20 (2013).
6. Caiazza, N. C., Shanks, R. M. & O'Toole, G. A. Rhamnolipids modulate swarming motility patterns of Pseudomonas aeruginosa. *J. Bacteriol.* **187**, 7351–7361 (2005).
7. Ahator, S. D. & Zhang, L. Small is mighty-chemical communication systems in Pseudomonas aeruginosa. *Annu. Rev. Microbiol.* **73**, 559–578 (2019).
8. Papenfort, K. & Bassler, B. L. Quorum sensing signal-response systems in Gram-negative bacteria. *Nat. Rev. Microbiol.* **14**, 576–588 (2016).
9. Lin, J., Cheng, J., Wang, Y. & Shen, X. The Pseudomonas Quinolone Signal (PQS): not just for quorum sensing anymore. *Front. Cell Infect. Microbiol.* **8**, 230 (2018).
10. Soh, E. Y. et al. Disruption of the Pseudomonas aeruginosa Tat system perturbs PQS-dependent quorum sensing and biofilm maturation through lack of the Rieske cytochrome bc1 sub-unit. *PLoS Pathog.* **17**, e1009425 (2021).
11. Rampioni, G. et al. Unravelling the genome-wide contributions of specific 2-Alkyl-4-Quinolones and PqsE to quorum sensing in Pseudomonas aeruginosa. *PLoS Pathog.* **12**, e1006029 (2016).
12. Florez, C., Raab, J. E., Cooke, A. C. & Schertzer, J. W. Membrane distribution of the pseudomonas quinolone signal modulates outer membrane vesicle production in Pseudomonas aeruginosa. *mBio* **8**. https://doi.org/10.1128/mBio.01034-17 (2017).
13. Yang, L., Nilsson, M., Gjermansen, M., Givskov, M. & Tolker-Nielsen, T. Pyoverdine and PQS mediated subpopulation interactions involved in Pseudomonas aeruginosa biofilm formation. *Mol. Microbiol.* **74**, 1380–1392 (2009).
14. Yang, L. et al. Effects of iron on DNA release and biofilm development by Pseudomonas aeruginosa. *Microbiology* **153**, 1318–1328 (2007).
15. Liu, X. et al. Cell division factor ZapE regulates Pseudomonas aeruginosa biofilm formation by impacting the pqs quorum sensing system. *mLife* **2**, 28–42 (2023).
16. Toyofuku, M., Schild, S., Kaparakis-Liaskos, M. & Eberl, L. Composition and functions of bacterial membrane vesicles. *Nat. Rev. Microbiol.* **21**, 415–430 (2023).
17. Colombo, M., Raposo, G. & Théry, C. Biogenesis, secretion, and intercellular interactions of exosomes and other extracellular vesicles. *Annu. Rev. Cell Dev. Biol.* **30**, 255–289 (2014).
18. Toyofuku, M., Nomura, N. & Eberl, L. Types and origins of bacterial membrane vesicles. *Nat. Rev. Microbiol.* **17**, 13–24 (2019).
19. Cooke, A. C., Nello, A. V., Ernst, R. K. & Schertzer, J. W. Analysis of Pseudomonas aeruginosa biofilm membrane vesicles supports multiple mechanisms of biogenesis. *PLoS ONE* **14**, e0212275 (2019).

20. Schwechheimer, C. & Kuehn, M. J. Outer-membrane vesicles from Gram-negative bacteria: biogenesis and functions. *Nat. Rev. Microbiol.* **13**, 605–619 (2015).
21. Hör, J., Gorski, S. A. & Vogel, J. Bacterial RNA biology on a genome scale. *Mol. Cell* **70**, 785–799 (2018).
22. Jia, T. et al. A novel small RNA promotes motility and virulence of enterohemorrhagic *Escherichia coli* O157:H7 in response to ammonium. *mBio.* **12**. https://doi.org/10.1128/mBio.03605-20 (2021).
23. Jia, T. et al. The phosphate-induced small RNA EsrL promotes E. coli virulence, biofilm formation, and intestinal colonization. *Sci. Signal.* **16**, eabm0488 (2023).
24. Dendooven, T., Sonnleitner, E., Bläsi, U. & Luisi, B. F. Translational regulation by Hfq-Crc assemblies emerges from polymorphic ribonucleoprotein folding. *Embo J.* **42**, e111129 (2023).
25. Gebhardt, M. J. et al. Hfq-licensed RNA-RNA interactome in Pseudomonas aeruginosa reveals a keystone sRNA. *Proc. Natl Acad. Sci. USA* **120**, e2218407120 (2023).
26. Wang, C., Ye, F., Kumar, V., Gao, Y. G. & Zhang, L. H. BswR controls bacterial motility and biofilm formation in Pseudomonas aeruginosa through modulation of the small RNA rsmZ. *Nucleic Acids Res.* **42**, 4563–4576 (2014).
27. Liu, P. et al. The function of small RNA in Pseudomonas aeruginosa. *PeerJ* **10**, e13738 (2022).
28. Sonnleitner, E. et al. The small RNA PhrS stimulates synthesis of the Pseudomonas aeruginosa quinolone signal. *Mol. Microbiol.* **80**, 868–885 (2011).
29. Reinhart, A. A. et al. The Pseudomonas aeruginosa PrrF small RNAs regulate iron homeostasis during acute murine lung infection. *Infect. Immun.* **85**. https://doi.org/10.1128/iai.00764-16 (2017).
30. Carver, T., Harris, S. R., Berriman, M., Parkhill, J. & McQuillan, J. A. Artemis: an integrated platform for visualization and analysis of high-throughput sequence-based experimental data. *Bioinformatics* **28**, 464–469 (2012).
31. Liu, J. H. et al. Bacmethy: a novel and convenient tool for investigating bacterial DNA methylation pattern and their transcriptional regulation effects. *Imeta* **3**, e186 (2024).
32. Pettersen, E. F. et al. UCSF chimera - A visualization system for exploratory research and analysis. *J. Comput. Chem.* **25**, 1605–1612 (2004).
33. Yan, Y. M., Zhang, D., Zhou, P., Li, B. T. & Huang, S. Y. HDOCK: a web server for protein-protein and protein-DNA/RNA docking based on a hybrid strategy. *Nucleic Acids Res.* **45**, W365–W373 (2017).
34. Seeliger, D. & de Groot, B. L. Ligand docking and binding site analysis with PyMOL and Autodock/Vina. *J. Comput. Aid Mol. Des.* **24**, 417–422 (2010).
35. Cai, Y. M. et al. The c-di-GMP Phosphodiesterase PipA (PA0285) regulates autoaggregation and Pf4 bacteriophage production in Pseudomonas aeruginosa PAO1. *Appl. Environ. Microbiol.* **88**, e0003922 (2022).
36. Belon, C. et al. A macrophage subversion factor is shared by intracellular and extracellular pathogens. *PLoS Pathog.* **11**, e1004969 (2015).
37. Ortori, C. A. et al. Simultaneous quantitative profiling of N-acyl-L-homoserine lactone and 2-alkyl-4(1H)-quinolone families of quorum-sensing signaling molecules using LC-MS/MS. *Anal. Bioanal. Chem.* **399**, 839–850 (2011).
38. Chao, Y. J. et al. In vivo cleavage map illuminates the central role of RNase E in Coding and Non-coding RNA pathways. *Mol. Cell* **65**, 39–51 (2017).
39. Winsor, G. L. et al. Enhanced annotations and features for comparing thousands of Pseudomonas genomes in the Pseudomonas genome database. *Nucleic Acids Res.* **44**, D646–D653 (2016).
40. Altschul, S. F., Gish, W., Miller, W., Myers, E. W. & Lipman, D. J. Basic local alignment search tool. *J. Mol. Biol.* **215**, 403–410 (1990).
41. Zou, L., Susko, E., Field, C. & Roger, A. J. Fitting nonstationary general-time-reversible models to obtain edge-lengths and frequencies for the barry-hartigan model. *Syst. Biol.* **61**, 927–940 (2012).
42. Zhang, Y. F. et al. Probing the sRNA regulatory landscape of P. aeruginosa: post-transcriptional control of determinants of pathogenicity and antibiotic susceptibility. *Mol. Microbiol.* **106**, 919–937 (2017).
43. Chao, Y., Papenfort, K., Reinhardt, R., Sharma, C. M. & Vogel, J. An atlas of Hfq-bound transcripts reveals 3' UTRs as a genomic reservoir of regulatory small RNAs. *Embo J.* **31**, 4005–4019 (2012).
44. Gill, E. E. et al. High-throughput detection of RNA processing in bacteria. *BMC Genom.* **19**, 223 (2018).
45. Stover, C. K. et al. Complete genome sequence of Pseudomonas aeruginosa PAO1, an opportunistic pathogen. *Nature* **406**, 959–964 (2000).
46. Van Gennip, M. et al. Inactivation of the rhlA gene in Pseudomonas aeruginosa prevents rhamnolipid production, disabling the protection against polymorphonuclear leukocytes. *Apmis.* **117**, 537–546 (2009).
47. Flemming, H. C. et al. Biofilms: an emergent form of bacterial life. *Nat. Rev. Microbiol.* **14**, 563–575 (2016).
48. Li, J. et al. Colistin: the re-emerging antibiotic for multidrug-resistant Gram-negative bacterial infections. *Lancet Infect. Dis.* **6**, 589–601 (2006).
49. Duan, X. et al. A bacterial Quorum sensing regulated protease inhibits host immune responses by cleaving death domains of innate immune adaptors. *Adv. Sci.* **10**, e2304891 (2023).
50. Bisht, K., Baishya, J. & Wakeman, C. A. Pseudomonas aeruginosa polymicrobial interactions during lung infection. *Curr. Opin. Microbiol.* **53**, 1–8 (2020).
51. Coleman, J. P. et al. Pseudomonas aeruginosa PqsA is an anthranilate-coenzyme A ligase. *J. Bacteriol.* **190**, 1247–1255 (2008).
52. Zhang, Y. M., Frank, M. W., Zhu, K., Mayasundari, A. & Rock, C. O. PqsD is responsible for the synthesis of 2,4-dihydroxyquinoline, an extracellular metabolite produced by Pseudomonas aeruginosa. *J. Biol. Chem.* **283**, 28788–28794 (2008).
53. Drees, S. L. et al. PqsBC, a condensing enzyme in the biosynthesis of the Pseudomonas aeruginosa Quinolone signal: crystal structure, inhibition, and reaction mechanism. *J. Biol. Chem.* **291**, 6610–6624 (2016).
54. Schertzer, J. W., Brown, S. A. & Whiteley, M. Oxygen levels rapidly modulate Pseudomonas aeruginosa social behaviours via substrate limitation of PqsH. *Mol. Microbiol.* **77**, 1527–1538 (2010).
55. Cao, H. et al. A quorum sensing-associated virulence gene of Pseudomonas aeruginosa encodes a LysR-like transcription regulator with a unique self-regulatory mechanism. *Proc. Natl Acad. Sci. USA* **98**, 14613–14618 (2001).
56. McGrath, S., Wade, D. S. & Pesci, E. C. Dueling quorum sensing systems in Pseudomonas aeruginosa control the production of the Pseudomonas quinolone signal (PQS). *FEMS Microbiol. Lett.* **230**, 27–34 (2004).
57. Diggle, S. P. et al. The Pseudomonas aeruginosa quinolone signal molecule overcomes the cell density-dependency of the quorum sensing hierarchy, regulates rhl-dependent genes at the onset of stationary phase and can be produced in the absence of LasR. *Mol. Microbiol.* **50**, 29–43 (2003).
58. Goh, Y. F. et al. Associational resistance to predation by protists in a mixed species biofilm. *Appl. Environ. Microbiol.* **89**, e0174122 (2023).

59. Campbell, E. A. et al. Structural mechanism for rifampicin inhibition of bacterial rna polymerase. *Cell* **104**, 901–912 (2001).
60. Ramirez-Peña, E., Treviño, J., Liu, Z., Perez, N. & Sumby, P. The group A Streptococcus small regulatory RNA FasX enhances streptokinase activity by increasing the stability of the ska mRNA transcript. *Mol. Microbiol.* **78**, 1332–1347 (2010).
61. Pfeiffer, V., Papenfort, K., Lucchini, S., Hinton, J. C. & Vogel, J. Coding sequence targeting by MicC RNA reveals bacterial mRNA silencing downstream of translational initiation. *Nat. Struct. Mol. Biol.* **16**, 840–846 (2009).
62. Mackie, G. A. & RNase, E. at the interface of bacterial RNA processing and decay. *Nat. Rev. Microbiol.* **11**, 45–57 (2013).
63. Turbant, F. et al. Interactions and insertion of *Escherichia coli* Hfq into outer membrane vesicles as revealed by infrared and orientated circular dichroism spectroscopies. *Int. J. Mol. Sci.* **24**. https://doi.org/10.3390/ijms241411424 (2023).
64. Turbant, F. et al. Unraveling membrane perturbations caused by the bacterial riboregulator Hfq. *Int. J. Mol. Sci.* **23**. https://doi.org/10.3390/ijms23158739 (2022).
65. Zavan, L. et al. The mechanism of Pseudomonas aeruginosa outer membrane vesicle biogenesis determines their protein composition. *Proteomics* **23**, e2200464 (2023).
66. Cornforth, D. M. et al. Pseudomonas aeruginosa transcriptome during human infection. *Proc. Natl Acad. Sci. USA* **115**, E5125–e5134 (2018).
67. Rossi, E., Falcone, M., Molin, S. & Johansen, H. K. High-resolution in situ transcriptomics of Pseudomonas aeruginosa unveils genotype independent patho-phenotypes in cystic fibrosis lungs. *Nat. Commun.* **9**, 3459 (2018).
68. Qu, J. et al. Persistent bacterial coinfection of a COVID-19 patient caused by a genetically adapted Pseudomonas aeruginosa chronic Colonizer. *Front. Cell Infect. Microbiol.* **11**, 641920 (2021).
69. Whiteley, M., Diggle, S. P. & Greenberg, E. P. Progress in and promise of bacterial quorum sensing research. *Nature* **551**, 313–320 (2017).
70. Valentini, M., Gonzalez, D., Mavridou, D. A. & Filloux, A. Lifestyle transitions and adaptive pathogenesis of Pseudomonas aeruginosa. *Curr. Opin. Microbiol.* **41**, 15–20 (2018).
71. Ferrara, S. et al. The small RNA ErsA plays a role in the regulatory network of Pseudomonas aeruginosa pathogenicity in airway infections. *mSphere* **5** (2020).
72. Reinhart, A. A. et al. The prrF-encoded small regulatory RNAs are required for iron homeostasis and virulence of Pseudomonas aeruginosa. *Infect. Immun.* **83**, 863–875 (2015).
73. Goodman, A. L. et al. A signaling network reciprocally regulates genes associated with acute infection and chronic persistence in Pseudomonas aeruginosa. *Dev. Cell* **7**, 745–754 (2004).
74. Moscoso, J. A., Mikkelsen, H., Heeb, S., Williams, P. & Filloux, A. The Pseudomonas aeruginosa sensor RetS switches type III and type VI secretion via c-di-GMP signalling. *Environ. Microbiol.* **13**, 3128–3138 (2011).
75. Chua, S. L. et al. Dispersed cells represent a distinct stage in the transition from bacterial biofilm to planktonic lifestyles. *Nat. Commun.* **5**, 4462 (2014).
76. Hör, J., Matera, G., Vogel, J., Gottesman, S. & Storz, G. Trans-acting small RNAs and their effects on gene expression in *Escherichia coli* and *Salmonella enterica*. *EcoSal Plus* **9**. https://doi.org/10.1128/ecosalplus.ESP-0030-2019 (2020).
77. Jagodnik, J., Brosse, A., Le Lam, T. N., Chiaruttini, C. & Guillier, M. Mechanistic study of base-pairing small regulatory RNAs in bacteria. *Methods* **117**, 67–76 (2017).
78. Hui, M. P., Foley, P. L. & Belasco, J. G. Messenger RNA degradation in bacterial cells. *Annu. Rev. Genet.* **48**, 537–559 (2014).
79. Djapgne, L. et al. The Pseudomonas aeruginosa PrrF1 and PrrF2 Small Regulatory RNAs Promote 2-Alkyl-4-Quinolone Production through Redundant Regulation of the antR mRNA. *J. Bacteriol.* **200**. https://doi.org/10.1128/jb.00704-17 (2018).
80. Heidrich, N., Moll, I. & Brantl, S. In vitro analysis of the interaction between the small RNA SR1 and its primary target ahrC mRNA. *Nucleic Acids Res.* **35**, 4331–4346 (2007).
81. Cao, P. et al. A Pseudomonas aeruginosa small RNA regulates chronic and acute infection. *Nature* **618**, 358–364 (2023).
82. Mugunthan, S. et al. RNA is a key component of extracellular DNA networks in Pseudomonas aeruginosa biofilms. *Nat. Commun.* **14**, 7772 (2023).
83. Aytar Çelik, P. et al. Bacterial membrane vesicle functions, laboratory methods, and applications. *Biotechnol. Adv.* **54**, 107869 (2022).
84. Flemming, H. C. et al. The biofilm matrix: multitasking in a shared space. *Nat. Rev. Microbiol.* **21**, 70–86 (2023).
85. Pérez-Cruz, C., Briansó, F., Sonnleitner, E., Bläsi, U. & Mercadé, E. RNA release via membrane vesicles in Pseudomonas aeruginosa PAO1 is associated with the growth phase. *Environ. Microbiol.* **23**, 5030–5041 (2021).
86. Lin, J. et al. A Pseudomonas T6SS effector recruits PQS-containing outer membrane vesicles for iron acquisition. *Nat. Commun.* **8**, 14888 (2017).
87. Kulp, A. & Kuehn, M. J. Biological functions and biogenesis of secreted bacterial outer membrane vesicles. *Annu. Rev. Microbiol.* **64**, 163–184 (2010).
88. Zhao, Z. et al. Regulation of the formation and structure of biofilms by quorum sensing signal molecules packaged in outer membrane vesicles. *Sci. Total Environ.* **806**, 151403 (2022).
89. Li, Y. et al. Self-organized canals enable long-range directed material transport in bacterial communities. *Elife* **11**. https://doi.org/10.7554/eLife.79780 (2022).
90. Koeppen, K. et al. A novel mechanism of host-pathogen interaction through sRNA in bacterial outer membrane vesicles. *PLoS Pathog.* **12**, e1005672 (2016).
91. Moriano-Gutierrez, S. et al. The noncoding small RNA SsrA is released by Vibrio fischeri and modulates critical host responses. *PLoS Biol.* **18**, e3000934 (2020).
92. Sahr, T. et al. Translocated Legionella pneumophila small RNAs mimic eukaryotic microRNAs targeting the host immune response. *Nat. Commun.* **13**, 762 (2022).

Acknowledgements

The authors would like to thank Prof. Chris Soon Heng Tan from the Department of Chemistry, Southern University of Science and Technology for help with the LC-MS/MS analysis and Prof. Lei Dai from Shenzhen Institutes of Advanced Technology for discussing the possibility of math models. TEM data were obtained using equipment maintained by Southern University of Science and Technology Core Research Facilities. This work was supported by the National Key Research and Development Program of China (2022YFC2304700); the National Natural Science Foundation of China (32300068, 32270196, 91951204, 32200155, 32200053, and 32300060); Guangdong Basic and Applied Basic Research Foundation (2019A1515110640 and 2020A1515010316); Shenzhen Science and Technology Program (KQTD20200909113758004); and Guangdong Pearl River Talent Plan.

Author contributions

T.J. and L.Y. designed the study. T.J., X.B., M.L., C.Z., S.L., and A.R. performed experiments. T.Z., Y.Z., Y.L., X. L., B.L., Y.D., and G.L. analyzed the results. T.J. and L.Y. drafted and revised the manuscript. All authors contributed to the article and approved the submitted version.

Competing interests
The authors declare no competing interests.

Additional information
Supplementary information The online version contains supplementary material available at https://doi.org/10.1038/s41522-024-00550-4.

Correspondence and requests for materials should be addressed to Liang Yang.